Mast cells regulate myofilament calcium sensitization and heart function after myocardial infarction

Anta Ngkelo,[1] Adèle Richart,[1] Jonathan A. Kirk,[2] Philippe Bonnin,[3] Jose Vilar,[1] Mathilde Lemitre,[1] Pauline Marck,[4] Maxime Branchereau,[4] Sylvain Le Gall,[1] Nisa Renault,[1] Coralie Guerin,[5] Mark J. Ranek,[2] Anaïs Kervadec,[1] Luca Danelli,[6,7,8] Gregory Gautier,[6,7] Ulrich Blank,[6,7,8] Pierre Launay,[6,7] Eric Camerer,[1] Patrick Bruneval,[1,9] Philippe Menasche,[1,9] Christophe Heymes,[4] Elodie Luche,[10] Louis Casteilla,[10] Béatrice Cousin,[10] Hans-Reimer Rodewald,[11] David A. Kass,[2] and Jean-Sébastien Silvestre[1]

[1]Institut National de la Santé et de la Recherche Médicale (INSERM), UMRS-970, Centre de Recherche Cardiovasculaire, Université Paris Descartes, Sorbonne Paris Cité, F-75015 Paris, France
[2]Division of Cardiology, Johns Hopkins Medical Institutions, Baltimore, MD 212015
[3]INSERM, U965, Hôpital Lariboisière–Fernand-Widal, Assistance Publique Hôpitaux de Paris, F-75010 Paris, France
[4]INSERM, UMR-1048, Institut des Maladies Métaboliques et Cardiovasculaires, F-31004 Toulouse, France
[5]National Cytometry Platform, Department of Infection and Immunity, Luxembourg Institute of Health, L-4354 Esch-sur-Alzette, Luxembourg
[6]Laboratoire d'Excellence INFLAMEX, Université Paris Diderot, Sorbonne Paris Cité, F-75018 Paris, France
[7]INSERM, U1149 and [8]Centre National de la Recherche Scientifique (CNRS) ERL 8252, F-75018 Paris, France
[9]Hôpital European George Pompidou, Assistance Publique Hôpitaux de Paris, F-75015 Paris, France
[10]STROMALab, Etablissement Français du Sang, INSERM U1031, CNRS ERL 5311, Université de Toulouse, F-31004 Toulouse, France
[11]Division of Cellular Immunology, German Cancer Research Center, D-69120 Heidelberg, Germany

Acute myocardial infarction (MI) is a severe ischemic disease responsible for heart failure and sudden death. Inflammatory cells orchestrate postischemic cardiac remodeling after MI. Studies using mice with defective mast/stem cell growth factor receptor c-Kit have suggested key roles for mast cells (MCs) in postischemic cardiac remodeling. Because c-Kit mutations affect multiple cell types of both immune and nonimmune origin, we addressed the impact of MCs on cardiac function after MI, using the c-Kit–independent MC-deficient (Cpa3^Cre/+) mice. In response to MI, MC progenitors originated primarily from white adipose tissue, infiltrated the heart, and differentiated into mature MCs. MC deficiency led to reduced postischemic cardiac function and depressed cardiomyocyte contractility caused by myofilament Ca^{2+} desensitization. This effect correlated with increased protein kinase A (PKA) activity and hyperphosphorylation of its targets, troponin I and myosin–binding protein C. MC-specific tryptase was identified to regulate PKA activity in cardiomyocytes via protease-activated receptor 2 proteolysis. This work reveals a novel function for cardiac MCs modulating cardiomyocyte contractility via alteration of PKA–regulated force–Ca^{2+} interactions in response to MI. Identification of this MC-cardiomyocyte cross-talk provides new insights on the cellular and molecular mechanisms regulating the cardiac contractile machinery and a novel platform for therapeutically addressable regulators.

Acute myocardial infarction (MI) is a severe ischemic disease responsible for sudden death and heart failure with prevalence rates rapidly increasing worldwide (White et al., 2014). The evolution in clinical practice has substantially reduced mortality and morbidity associated with this condition. However, given the adverse hemorrhagic effects of the integration of antithrombotic therapy and the high socioeconomic burden of ischemic heart disease, a need for novel effective targets

is emerging (White and Chew, 2008). Hence, efforts are directed toward pivotal pathways shaping cardiac homeostasis such as the inflammatory cellular responses (Zouggari et al., 2013; Boag et al., 2015; de Couto et al., 2015) as well as the molecular mechanisms that drive cardiac contractile function (Gorski et al., 2015; Movsesian, 2015).

Substantial interest has been drawn on the role of cardiac mast cells (MCs) in mediating postischemic adverse myocardial remodeling (Kritikou et al., 2016). MCs are innate immune cells, characterized morphologically by numerous cytoplasmic granules that contain a variety of mediators such as proteoglycans, histamine, proteases (chy-

The Rockefeller University Press $30.00
J. Exp. Med. 2016 Vol. 213 No. 7 1353–1374
www.jem.org/cgi/doi/10.1084/jem.20160081

1353

mase and tryptase), and proinflammatory cytokines that are released upon MC activation to influence the local tissue microenvironment (Wernersson and Pejler, 2014). To date, several studies investigating the role of MCs in cardiac function and remodeling have been contradicting (Janicki et al., 2015), which may relate to the use of c-Kit mutant mice (the c-kit W/Wv [Kitamura et al., 1978]) and the more recent Kit W-sh/W-sh mice (Kitamura et al., 1978; Grimbaldeston et al., 2005) with mutations in the gene encoding the receptor tyrosine kinase c-Kit with subsequent MC deficiency. Because deficient c-Kit signaling affects other lineages, including hematopoietic stem cells, progenitor cells, red blood cells, neutrophils, cardiomyocytes, melanocytes, and germ cells (Katz and Austen, 2011), it remains ambiguous to what extent MC absence is responsible for the observed phenotypes. Therefore, the distinct role of MCs, independently of c-Kit functions, on regulating postischemic cardiac remodeling and function is unknown.

Here we addressed the role of MCs in regulating cardiac function and contractility in response to acute MI by using the recently developed "Cre-mediated MC eradication" (Cre-Master or Cpa3$^{cre/+}$) mouse model, which yields constitutive and c-Kit–independent MC deficiency (Feyerabend et al., 2011). We show that MCs play a key role in regulating cardiomyocyte contractility and subsequently cardiac function after MI. We describe an MC-dependent mechanism of protein kinase A (PKA) activity and myofilament protein phosphorylation through MC-released tryptase.

RESULTS

MCs accumulate in the heart at day 7 after MI

To investigate the kinetics of mature MC infiltration after MI, digested infarcted tissue underwent flow cytometry/imaging analysis. Mature MCs were identified as c-kit$^+$FcεRI$^+$ by flow cytometry (Fig. 1 A), and the combination of these markers' expression was verified as corresponding to the typical granulated morphology of MCs by the side scatter light imaging on ImageStream (Fig. 1 B). MC numbers in the sham-operated hearts were very low, but a significant accumulation of MCs was observed at day 7 after MI (infarct: 30,341 ± 2,600 cells/g of tissue vs. sham: 628 ± 218 cells/g of tissue, P = 0.0025; Fig. 1 C). This was followed by a progressive decrease in MC numbers from day 10 until day 21 (Fig. 1 C). Based on metachromatic toluidine blue (TB) staining (Tallini et al., 2009), 91.3 ± 4.1% of cardiac MCs were degranulated at day 7 after MI (Fig. 1, D and E). In addition, there was a significant increase in the mRNA expression of mouse MC chymase (mMCP4) and tryptase (mMCP6) starting and/or peaking at day 7 in the infarcted myocardium (vs. sham-operated myocardium; Fig. 1, F and G), consistent with the connective tissue MC phenotype (CTMC; Forman et al., 2006). c-Kit$^+$tryptase$^+$ cells were also identified in human biopsies from coronary artery bypass surgery (not depicted).

MC progenitors (MCPs) are recruited into the heart and give rise to mature MCs in a stem cell factor (SCF)–dependent manner

Mature MCs increase at tissue sites by infiltration of precursors from the peripheral blood and reach differentiation/maturation by locally secreted growth factors (Welker et al., 2000). To assess whether this is the case in response to MI, we identified MCPs as Lin$^-$CD45$^+$CD34$^+$β7-integrin$^+$FcγRII/III$^+$ cells (Fig. 2 A; Chen et al., 2005; Schmetzer et al., 2016) and monitored their numbers in the BM, white adipose tissue (WAT), heart (Fig. 2, B–D), blood, and spleen (Fig. 2, J and K). MCPs increased significantly in numbers in the BM at days 3–5 and the WAT at day 3 in response to infarction (Fig. 2, B and C). In the infarcted heart, an accumulation of MCPs was observed at day 3 (infarct: 2,600 ± 600 cells/g vs. sham: 506 ± 215 cells/g of tissue, P = 0.017) that persisted until day 5 (Fig. 2 D). To evaluate whether the increase in MCP density in the heart is a result of local cardiac proliferation, BrdU incorporation was measured at days 3, 5, and 7 after infarction. A significant increase in BrdU-labeled MCPs was observed at day 5, 24 h after cumulative BrdU injections, with 2.8 ± 0.3% of the MCP cells being in a proliferative state (P = 0.007 vs. 0.27 ± 0.07% of BrdU$^+$ MCPs on day 3; Fig. 2, E and F). The c-kit ligand SCF is responsible for the proliferation of MCPs both in vitro (Kirshenbaum et al., 1992) and in vivo (Matsuzawa et al., 2003) and can be produced by several tissue-resident cells, such as fibroblasts, endothelial cells, and cardiac stem cells (Guo et al., 2009; Xiang et al., 2013). SCF mRNA levels significantly increased in the peri-infarcted tissue at day 5 after MI compared with sham-operated mice (Fig. 2 G). Neutralization of SCF by the systemic administration of an anti–SCF antibody (Oliveira et al., 2002) reduced proliferation and numbers of MCPs at day 5 after MI (Fig. 2 H) as well as numbers of mature MCs at day 7 after MI (SCF antibody: 0.01 ± 0.001% vs. rabbit serum: 0.03 ± 0.005% of c-kit$^+$FcεRI$^+$ cells, P = 0.026; Fig. 2 I). MCPs were also detectable in the blood circulation, but numbers were too low to draw conclusions on their kinetics of circulation (Fig. 2 J). Similarly, no significant differences were obtained in the splenic MCP numbers in response to MI (Fig. 2 K).

MCs preserve cardiac function after MI

We next evaluated the functional effect of MC accumulation in the infarcted myocardium by evaluating cardiac function 2 wk after infarction in the MC-eradicated Cpa3$^{cre/+}$ mice, which are selectively deficient for mature MCs (Feyerabend et al., 2011). c-kit$^+$FcεRI$^+$ cells were absent in the heart of Cpa3$^{cre/+}$ mice at day 7 after the infarct, as confirmed both by flow cytometry and TB staining–assisted counting (Fig. 3, A and B). Heart function of Cpa3$^{cre/+}$ mice was comparable with WT mice when sham operated. However, postinfarcted hearts lacking MCs displayed a significantly lower shortening fraction (SF [SF%]; Erdei et al., 2004; WT 28.15 ± 1.7% SF vs. Cpa3$^{cre/+}$: 17.27 ± 1.9% SF, P = 0.0043; Fig. 3 C). In addition, the left ventricular internal postsystolic diameter was significantly
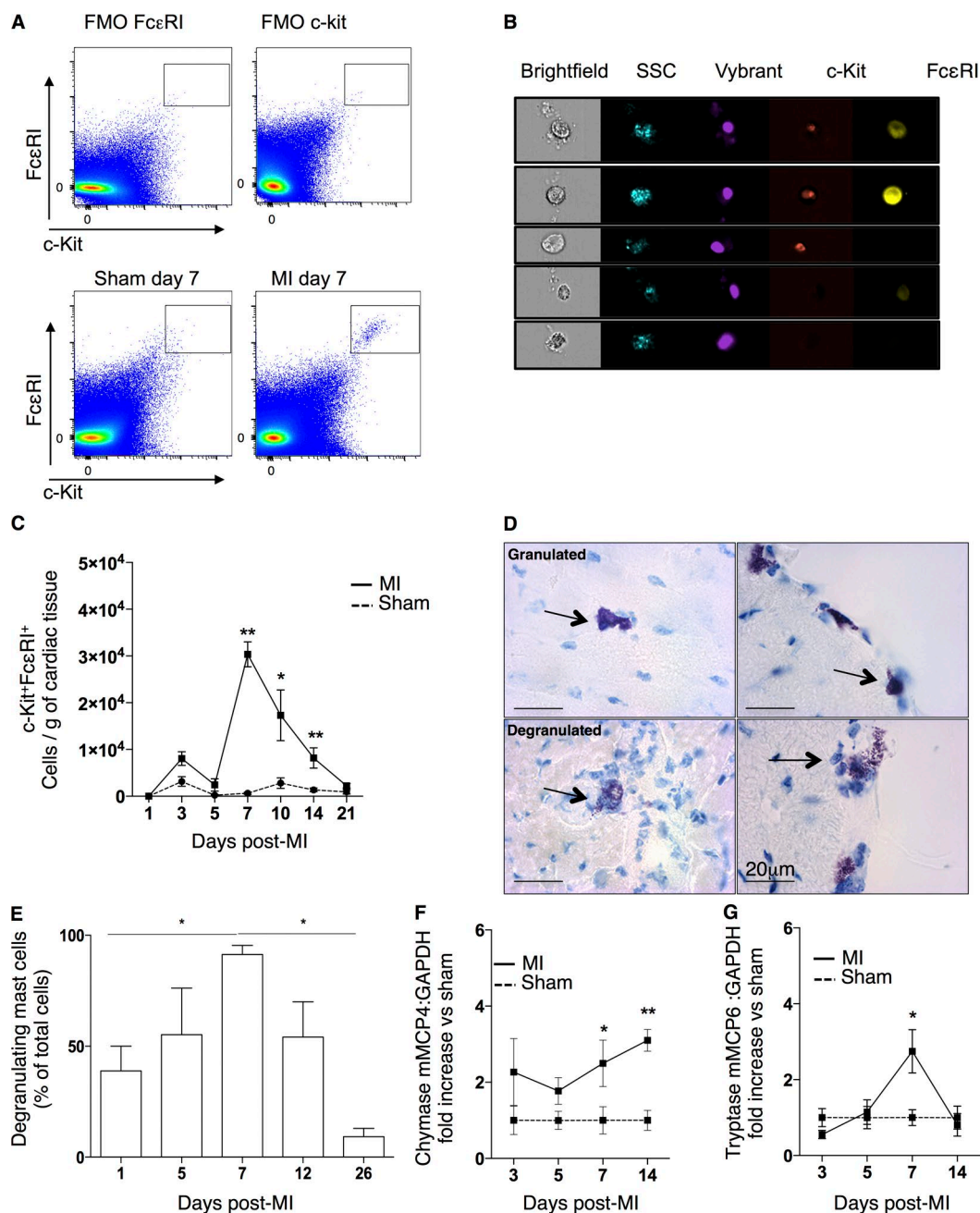
1354

The role of mast cells in myocardial infarction | Ngkelo et al.

Figure 1. **Characterization of cardiac mature MCs after MI.** (A and B) Representative fluorescence minus one control (FMO) and flow cytometry gating for mature cardiac MCs (c-kit⁺FcεRI⁺) at day 7 in sham-operated and infarcted myocardium (A) and representative image of ImageStream flow cytometer showing the morphology of Vybrant⁺c-kit⁺FcεRI⁺ cells under brightfield and side scatter (SSC) imaging with corresponding negative controls (B). (C) Time-dependent monitoring cardiac mature MCs/gram of cardiac tissue in response to infarction ($n = 4–8$, two independent experiments). *, $P < 0.05$; **, $P < 0.01$. Kruskal–Wallis and Dunn's post hoc test for comparisons for sham versus MI at different time points. (D) Representative cardiac TB staining of mature MCs at granulated (above) and degranulated (below) states found both in the myocardium (left) and at the periphery (right). Arrows point to representative cardiac MCs. (E) Cardiac degranulated cells as the percentage of total cells counted by TB staining ($n = 6$, two independent experiments). *, $P < 0.05$. Kruskal–Wallis and Dunn's post hoc test for comparisons at different time points. (F and G) Cardiac mRNA expression of chymase mMCP4 and tryptase mMCP6 at different time points after the sham operation or infarction ($n = 6–8$). *, $P < 0.05$; **, $P < 0.01$. Kruskal–Wallis and Dunn's post hoc test for comparisons for sham versus MI at different time points. All data shown are representative of at least three independent experiments. All values are presented as mean ± SEM. Sham, sham-operated animals.
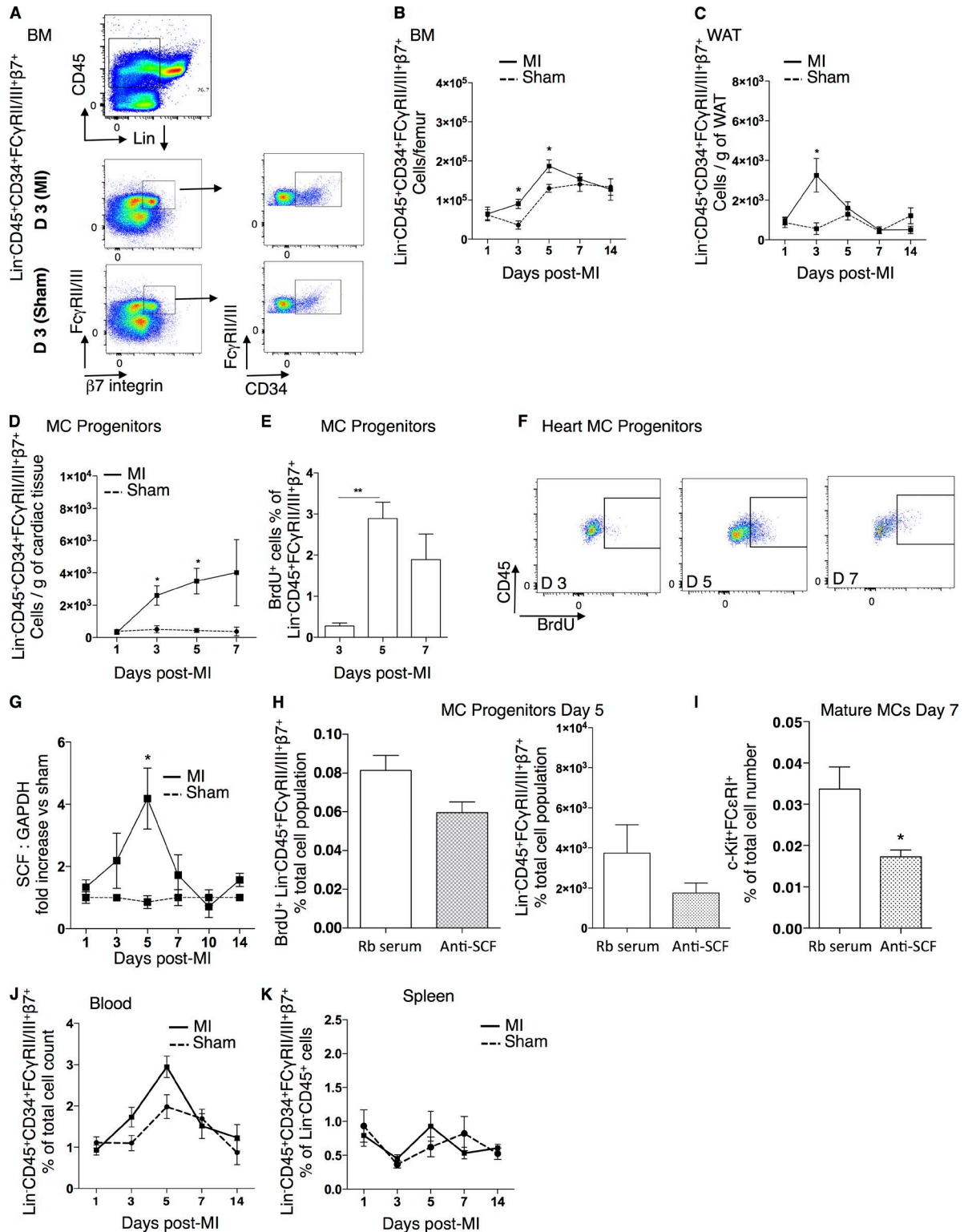
Figure 2. **SCF–dependent accumulation of cardiac mature MCs.** (A) Representative flow cytometry gating for MCPs (Lin⁻CD45⁺CD34⁺β7-integrin⁺FCγRII/III⁺) in the BM of sham-operated mice versus mice with MI at day 3. (B and C) Time-dependent increase of MCPs at days 3 and 5 after MI in the BM (B) and at day 3 in WAT (C) compared with sham control mice ($n = 4$–9, two independent experiments). *, $P < 0.05$, Kruskal–Wallis and Dunn's post hoc test for comparisons of sham versus MI at different time points. (D) Numbers of MCPs/gram of cardiac tissue after infarct versus sham-operated mice ($n = 4$–9, two independent experiments). *, $P < 0.05$, Kruskal–Wallis and Dunn's post hoc test for comparisons of sham versus MI at different time points. (E) Increased

increased in Cpa3[cre/+] compared with WT mice after infarction. No significant differences were observed between the two groups in left ventricular end-diastolic internal diameter (Fig. 3 C) or heart rate (not depicted). Left ventricular posterior wall end-diastolic thickness and interventricular end-diastolic septal diameter were also decreased in Cpa3[cre/+] compared with WT mice (not depicted).

To identify the cause of reduced heart function in the MC-deficient mice, we evaluated inflammation and cardiac remodeling after infarction. There was no difference in the levels of collagen deposition, infarct size, capillary density, cardiomyocyte size, and number, as well as in the amount of apoptotic resident cells in the Cpa3[cre/+] mice compared with WT mice in response to infarction (Fig. 3, D and E). In line with these results, we found no differences in the numbers of recruited monocytes, macrophages, B lymphocytes, and CD8^{+} and CD3^{+} T lymphocytes to the infarcted heart in Cpa3[cre/+] in response to MI compared with WT mice (Fig. 4 A). Accordingly, we assessed the release of key inflammatory mediators in the infarcted heart, including CCL2, CCL7, IL-6, IL-1β, and TNF, and found no difference in the Cpa3[cre/+] mice compared with WT mice at all time points tested (Fig. 4 B).

Cardiac remodeling in c-Kit W/Wv and disodium cromoglycate (DSCG)–treated mice after MI

Accumulation of cardiac MCs after infarction was SCF dependent, and a high percentage of cardiac MCs were degranulated in the infarcted heart. To assess whether these mechanisms are involved in the MC-dependent decline in cardiac function after the infarct, we used two widely studied animal models: the c-Kit W/Wv mice and systemic treatment with the degranulation inhibitor DSCG (Zhang et al., 2016). Both animal models are associated with impaired MC function and have been extensively used to investigate the biological role of MCs in a broad range of disease pathologies (Kovanen, 2009; He and Shi, 2013). We first assessed the number of cardiac MCs by TB staining after infarct in both mouse models. c-Kit W/Wv mice were MC poor but not completely deficient after MI, consistent with another report where inflammatory signaling can reverse MC absence in these mice (Feyerabend et al., 2011), and as expected, DSCG treatment did not affect cardiac MC density (Fig. 5 A). We next evaluated cardiac function at 2 wk after MI and found a significant reduction in left ventricular ejection fraction (EF)

in both DSCG-treated (16.3 ± 1.6% EF) and c-Kit W/Wv mice (20 ± 2.5% EF) compared with their respective controls and littermates (PBS: 30.2 ± 2.8% EF, c-Kit^{+/+}: 25.5 ± 4.6% EF; Fig. 5 B). However, in contrast with the Cpa3[cre/+] mice, there were significant differences in cardiac remodeling of these animal models of MC-impaired function. DSCG treatment had no effect on the infarct size, capillary density, or cardiomyocyte size but significantly increased levels of cardiac interstitial fibrosis and cell apoptosis (Fig. 5, C and D). In contrast, the c-Kit W/Wv mice had a significant increase in the number of cardiac apoptotic cells after MI but no difference in the rest of the remodeling parameters evaluated (Fig. 5, C and D). Because remodeling parameters were unaffected in the MC-eradicated Cpa3[cre/+] mice, we conclude that MCs preserve heart function after infarction but do not directly regulate cardiac remodeling.

Post-MI cardiac MCs originate primarily from the WAT

Most studies on MC origin, circulation, and maturation are focused on BM-derived MCPs (Chen et al., 2005; Franco et al., 2010), but a recent study by Poglio et al. (2010) identified the WAT as a reservoir of progenitor MCs that do not originate from the BM and are able to home to peripheral tissues. Because we observed increased numbers of MCPs in both the WAT and the BM at days 3 and 5 (Fig. 2), we next identified the primary source of origin of cardiac MCs after infarction. We transplanted lethally irradiated C57BL/6 mice with BM-derived cells from WT and Cpa3[cre/+] mice. SF% in WT mice reconstituted with Cpa3[cre/+]–derived BM cells was comparable with the SF% of WT animals reconstituted with BM-WT as measured 2 wk after the infarct (Fig. 6 A). In this line, reconstitution of WT mice with Cpa3[cre/+]–derived BM cells did not lead to absence of mature cardiac MCs after infarction, and conversely, reconstitution of Cpa3[cre/+] mice with WT-derived BM cells did not reverse the absence of mature MCs in the Cpa3[cre/+] mice after infarction (Fig. 6 B). Poglio et al. (2010) developed a competitive repopulation assay for assessing the function of WAT hematopoietic stem/progenitor cells (HSPCs) in comparison with BM competitor cells. WAT HSPCs (previously described as c-Kit[+]Lin[−]Sca[+]; Poglio et al., 2012) were FACS sorted from CD45.2 Cpa3[cre/+] mice or CD45.2 red MC and basophil mice (RMB), where the 3′-UTR of the Ms4a2 gene encoding the FcεRIβ chain includes a cassette composed of a sequence coding for the bright td-Tomato (tdT) fluorescence protein (Dahdah et al.,

proliferation of cardiac MCPs at day 5 of infarct, 24 h after BrdU administration ($n = 8$, two independent experiments). **, $P < 0.01$, Kruskal–Wallis and Dunn's post hoc test for comparisons at different time points. (F) Representative flow cytometry analysis of BrdU[+] MCPs at days 3, 5, and 7 after infarct. (G) mRNA expression of SCF in the cardiac tissue in response to infarction (vs. sham) peaking at day 5 ($n = 5$–10, two independent experiments). *, $P < 0.05$, Kruskal–Wallis and Dunn's post hoc test for comparisons of sham versus MI at different time points. (H) No significant effect of SCF antibody treatment on proliferation (left) and number (right) of CD45^{+}β7-integrin^{+}FCγRII/III^{+} cells at day 5 after MI ($n = 6$–8, two independent experiments). Mann–Whitney test for comparisons between groups. (I) SCF antibody reduced total numbers of mature MCs at day 7 after MI ($n = 6$–8, two independent experiments). *, $P < 0.05$, Mann–Whitney test for comparisons between groups. (J and K) MCPs (Lin^{−}CD45^{+}CD34^{+}FCγRII/III^{+}β7^{+}) were identified circulating in the blood (J) at low percentages and in the spleen (K) with no statistically significant changes in response to MI. Kruskal–Wallis and Dunn's post hoc test for comparisons of sham versus MI at different time points. All values are presented as mean ± SEM. anti, antibody against; D, day; Rb, rabbit; Sham, sham-operated animals.
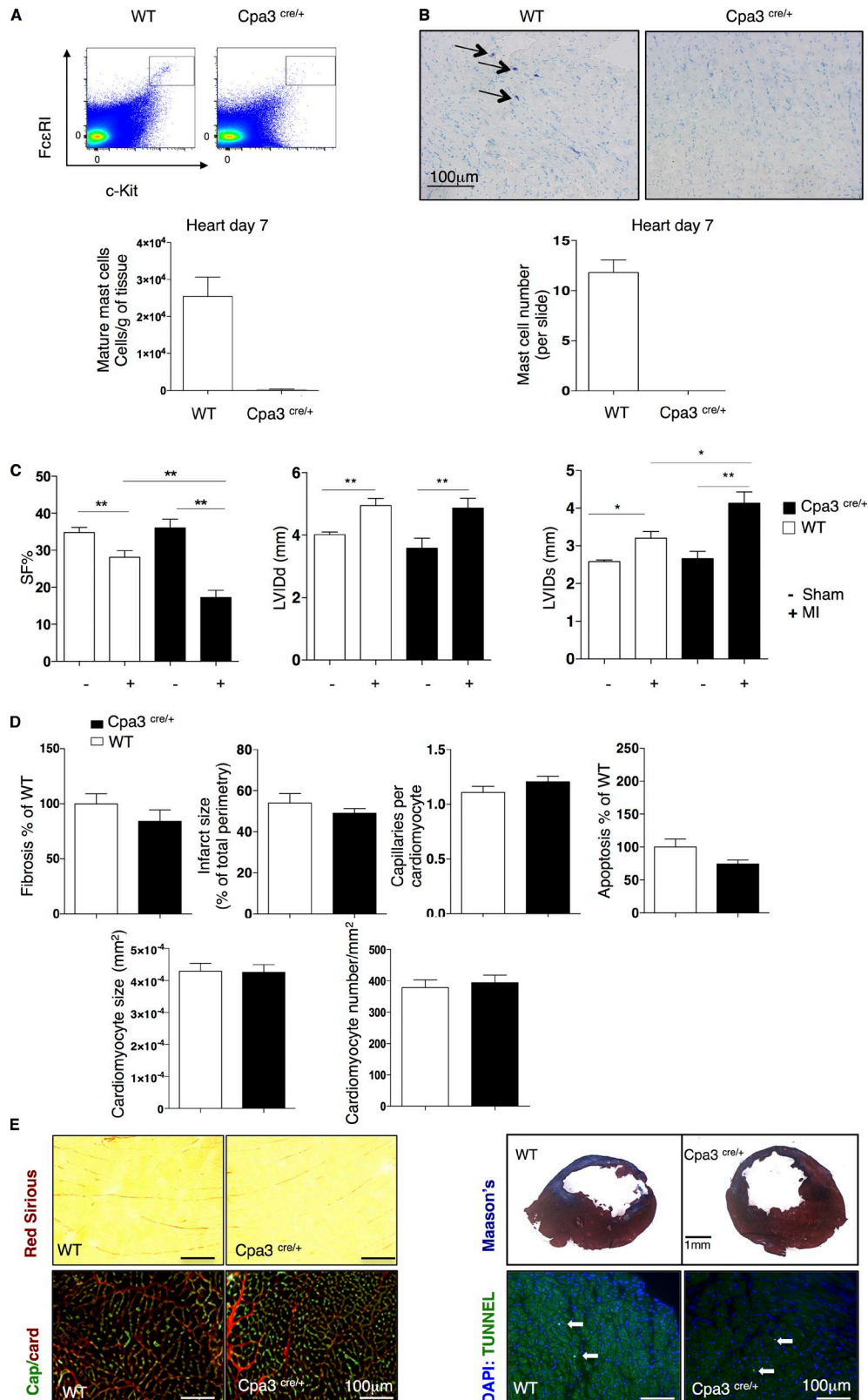
Figure 3. **Depressed cardiac function after MI in Cpa3^{cre/+} MC–deficient mice.** (A) Representative flow cytometry gating of c-kit⁺FcεRI⁺ cells in WT that are absent in Cpa3^{cre/+} mice at day 7 after MI (top); bar graphs show the numbers of mature MCs/gram of cardiac tissue (bottom; *n* = 5–8, two independent experiments). (B) Representative cardiac TB staining (top) and quantitative evaluation of mature MCs in infarcted heart (*n* = 5–6, two independent

2014). Lethally irradiated CD45.1 mice were cotransplanted with 2×10^3 WAT HSPC CD45.2$^+$ and 2×10^5 BM CD45.1$^+$ cells. WAT-HSPCs do not contain mature MCs (Fig. 6 C). Chimerism in the WAT was confirmed at 8 wk after transplantation by flow cytometry with a percentage of 20–30% of CD45.2$^+$ cells present (Fig. 6 D). Because WAT-HSPCs do not reconstitute hematopoietic organs (Poglio et al., 2012), chimerism in the BM was very low (Fig. 6 D). Transplantation of WT mice with WAT HSPCs from Cpa3$^{cre/+}$ mice significantly reduced SF% after MI (WT WAT donor: 33.3 ± 3.2% SF vs. Cpa3$^{cre/+}$ WAT donor: 21.7 ± 1.8% SF, P = 0.026; Fig. 6 E). In addition, no significant differences were found in BM and WAT transplanted mice on infarct size, capillary density, or fibrosis at day 14 after infarction (Fig. 6, A and E). To further investigate the origin of MCs, we compared the levels of tdT$^+$c-Kit$^+$ cells in WT mice transplanted either with both WAT-HSPCs from WT mice and BM cells from RMB mice or with both WAT-derived HSPCs from RMB mice and WT mice–derived BM cells. Similar numbers of c-Kit$^+$FcεRI$^+$ cells were observed in the heart at day 7 after infarction, regardless of the origin of transplanted cells. However, when tdT staining was used to monitor their origin, the mice transplanted with RMB-BM cells had significantly less tdT$^+$c-Kit$^+$ cells in the infarcted myocardium at day 7 after MI compared with WT mice transplanted with RMB-WAT cells (P = 0.0317; Fig. 6, F–H). Collectively, although MCPs were detectable both in the BM and the WAT (Fig. 2), WAT-derived MCPs appeared to be more efficient in homing toward the cardiac tissue after MI.

Cardiac MCs regulate myofilament sensitization to Ca^{2+}

MC eradication had negative effects on the cardiac function after infarction with decreased systolic left ventricular diameter. There was no difference in infarct size or cardiac remodeling in the hearts of Cpa3$^{cre/+}$ mice, suggesting a more direct impact on the myocardial contractile function. To further elucidate this MC-specific cardiac response, we examined the function and contractility properties of cardiomyocytes in the MC-depleted myocardial environment 14 d after the infarct. First, we assessed cardiomyocyte shortening (%) in response to field stimulation (1, 2, and 4 Hz). As shown in Fig. 7 A, MC deficiency significantly depressed the frequency response of left ventricular cardiomyocytes (Cpa3$^{cre/+}$: 6.08 ± 0.5% vs. WT: 8.8 ± 0.8% 2Hz; P = 0.009). Absence of MCs in the infarcted myocardium led to abnormal contraction and relaxation kinetics of the left ventric-

ular cardiomyocytes (Fig. 7 B), but there was no effect on the amplitude of Ca^{2+} transient peak in electrically stimulated cardiomyocytes (Fig. 7 C). In addition, sarcoplasmic reticulum load was maintained, indicating that Ca^{2+} influx and efflux were unaffected by MC eradication (Fig. 7 D). To further investigate contractile function, we determined myofilament force–Ca^{2+} dependence of left ventricular endocardial skinned myocytes at a steady-state (at day 14 after infarct). This dependence was markedly reduced in WT infarcted hearts compared with sham-operated hearts with maximum Ca^{2+}-activated force (F$_{max}$) declining nearly 50% (sham: 42.3 ± 0.5 mN/mm^2 vs. infarct: 19.8 ± 3.5 mN/mm^2, P = 0.0062; Fig. 7, E and F). Similar reduction in F$_{max}$ was exhibited by the myocytes from Cpa3$^{cre/+}$ mice (sham: 35.9 ± 2.4 mN/mm^2 vs. infarct: 19.2 ± 4.4 mN/mm^2, P = 0.0186; Fig. 7, E and F). Although F$_{max}$ and Hill coefficient remained unchanged between WT and Cpa3$^{cre/+}$ infarcted hearts, skinned myocytes from the MC-deficient ventricular environment displayed Ca^{2+} desensitization, as quantified by an increase in EC$_{50}$ (Ca^{2+} required to achieve 50% maximal force; WT: 2.8 ± 0.09 μM vs. Cpa3$^{cre/-}$: 3.5 ± 0.11 μM, P = 0.007; Fig. 7, E–H).

MC–dependent Ca^{2+} sensitization is mediated by myofilament phosphorylation

Ca^{2+} sensitivity is regulated by phosphorylation of several sarcomeric proteins involved in the regulation of actomyosin interactions, including cardiac troponin I (cTnI) and myosin-binding protein C (MyBPC), both catalyzed by PKA (Layland et al., 2005; Stelzer et al., 2007). We evaluated the phosphorylation levels of cTnI and MyBPC at residues known to confer a negative effect on Ca^{2+} sensitization in the mouse myocardium (Chen et al., 2010). Myofilament phosphorylation in response to infarction was significantly higher in the peri-infarcted cardiac tissue of Cpa3$^{cre/+}$ mice compared with WT mice both on cTnI (Ser22/23) and on MyBPC (Ser282 and Ser273) in a time-dependent manner, being observed 14 d after MI (but not at day 7; Fig. 8, A–C). This hyperphosphorylation event correlated with an increased activity of PKA in the Cpa3$^{cre/+}$ peri-infarcted area compared with WT mice at day 14 after infarction (WT infarct: 1.2 ± 0.07% vs. Cpa3$^{cre/+}$ infarct: 2.3 ± 0.2%, P = 0.0005; Fig. 8 D) that was not exhibited by the sham-operated cardiac tissue.

experiments). Arrows point to representative cardiac MCs. (C) Left ventricular %SF, LVIDd (left ventricular internal end-diastolic diameter), and LVIDs (left ventricular internal end-systolic diameter) measurements showing significant reduction of cardiac function (day 14) in Cpa3$^{cre/+}$ infarcted mice compared with WT (Cpa3$^{+/+}$) infarcted mice, with no differences on basal heart function (n = 6–7, two independent experiments). *, P < 0.05; **, P < 0.01, Kruskal–Wallis and Dunn's post hoc test for comparisons between groups. (D) Cardiac fibrosis, infarct size, capillaries' density, percentage of cell apoptosis, cardiomyocyte size, and number after infarction (day 14) in WT and Cpa3$^{cre/+}$ mice (n = 6–7, two independent experiments). (E) Representative images used for quantification of fibrosis, capillary density, infarct size, and density of apoptotic cardiac cells. Arrows point to representative apoptotic cells. All values are presented as mean ± SEM. Sham, sham-operated animals; WT, Cpa$^{+/+}$ littermates.
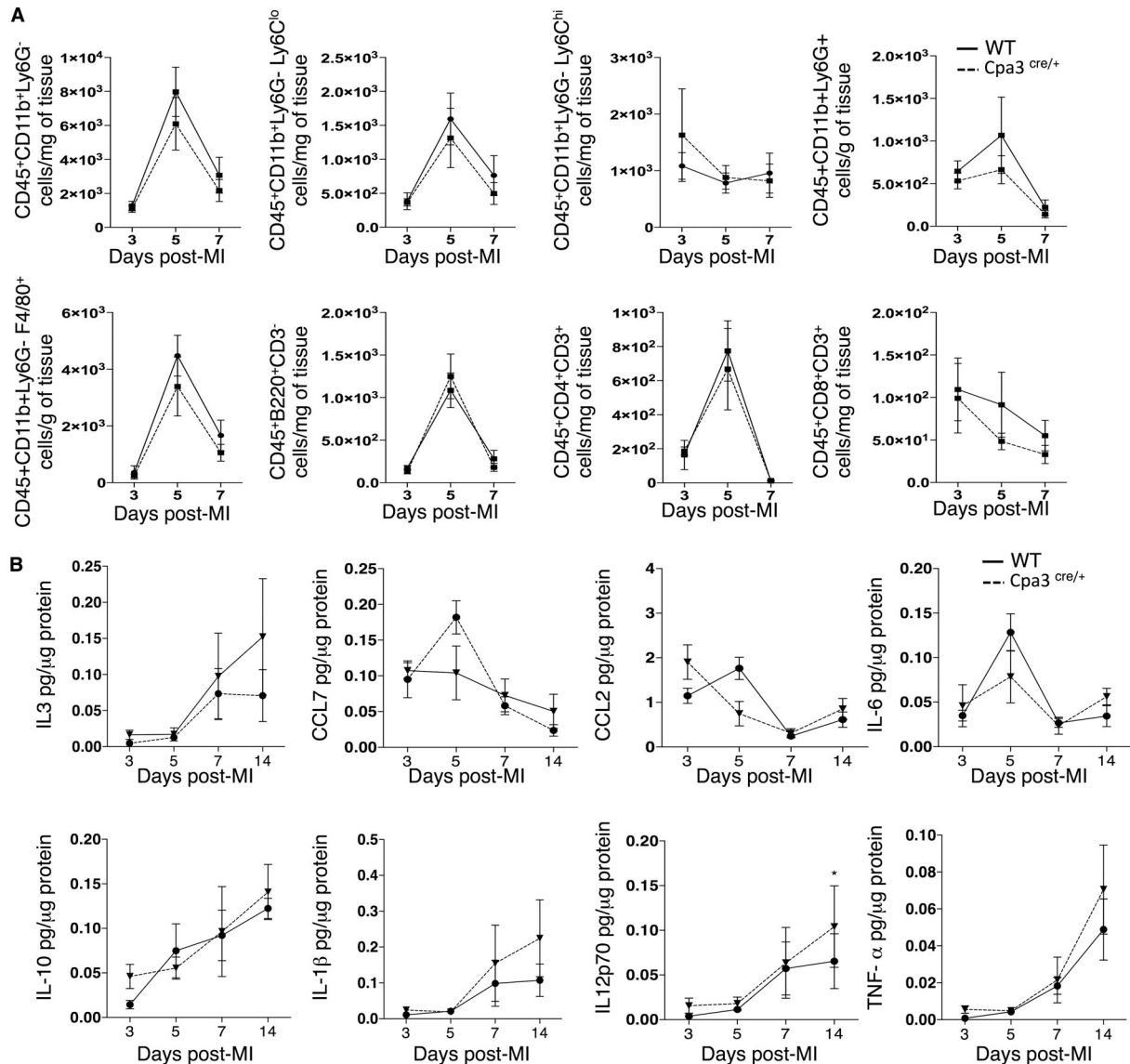
Figure 4. **Cpa3^cre/+ mice have a normal inflammatory response after MI.** (A) Inflammatory cell density (monocytes, macrophages, and B and T lymphocytes) in Cpa3^cre/+ mice was comparable with that of WT mice at days 3, 5, and 7 after MI (n = 7–8, two independent experiments). (B) Inflammatory mediators' concentration (IL3, CCL7, CCL2, IL-6, IL-10, IL-1β, IL12p70, and TNF; pg/μg of protein) was analyzed by FlowCytomix, and no differences were observed between WT and Cpa3^cre/+ mice at days 3, 5, 7, and 14 after MI (n = 6–8, 2 independent experiments). All values are presented as mean ± SEM. WT, Cpa^+/+ littermates.

Identification of tryptase-induced protease-activated receptor 2 (PAR2) activation as a mechanism of MC-regulated PKA activity

Because MC absence leads to increased PKA activity, we hypothesized that activation of a Gi-coupled protein receptor by an MC-released mediator could be involved. PAR2 can be cleaved by trypsin-like proteases such as MC tryptase (McLarty et al., 2011; Weithauser and Rauch, 2014), leading to the activation of Gi and consequential inhibition of the adenylyl cyclase–c-AMP–PKA axis (Sriwai et al., 2013). We analyzed the PAR2 cleaving capacity of both MC-specific

tryptase and chymase that are all absent in the hearts of the Cpa3^cre/+ mice after infarct (not depicted). Although MC chymase (mMCP4) cleaved PAR2, cleavage was not sensitive to replacement of arginine 36 of the canonical cleavage site with glycine (Fig. 8 E) and therefore unlikely to be signaling productive. Moreover, cardiac function at day 14 after infarction in mMCP4^−/− mice was comparable with WT mice as analyzed by echocardiography (not depicted). In contrast, tryptase showed canonical PAR2 cleavage consistent with receptor activation (Fig. 8 F). We next investigated whether tryptase-induced PAR2 cleavage could regulate intracellular
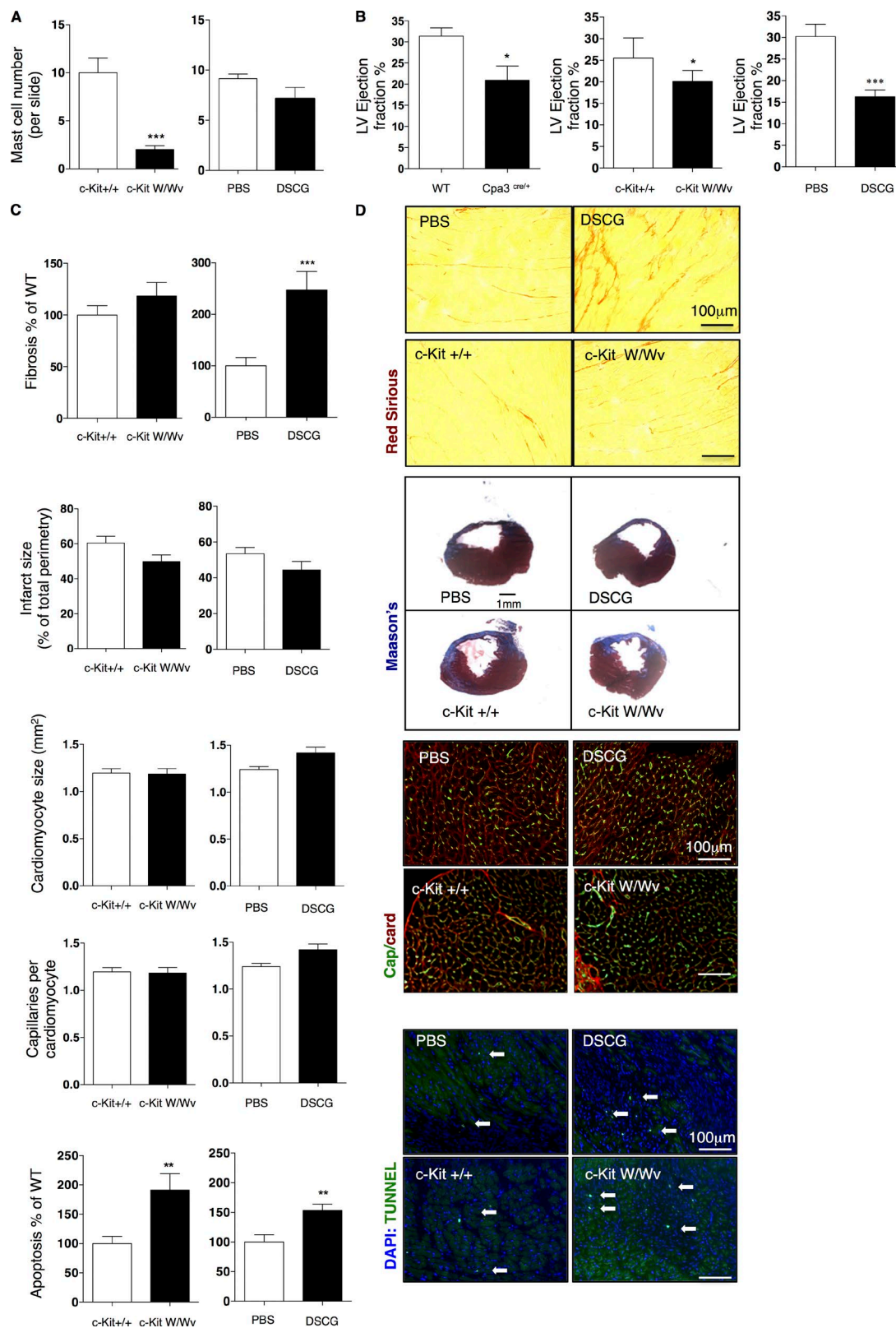
Figure 5. **Cardiac function and remodeling in c–KitW/Wv and DSCG–treated mice.** (A) TB-assisted MC counting in c-Kit W/Wv and DSCG-treated mice compared with their controls (c-Kit^{+/+} and PBS treated, respectively) on 5-µm slide sections (n = 6). (B) Reduced left ventricular (LV) cardiac function (EF%) at day 14 after MI in Cpa3[Cre/+], DSCG-treated animals and c-Kit W/Wv compared with their respective controls (n = 6). (C) Evaluation of cardiac

PKA activity in cardiomyocytes. As shown in Fig. 8 G, IBMX-induced PKA activation in H9C2 cells was attenuated by a PAR2-activating peptide (PAR2-AP; P = 0.04), which is known to activate Gi (Sriwai et al., 2013). Consistent with PAR2 cleavage, treatment with MC tryptase also significantly inhibited IBMX-induced PKA activity (P = 0.03). Because Cpa3$^{cre/+}$ mice express very low levels of tryptase mRNA (not depicted), we assessed whether the tryptase signaling is responsible for reduced cardiac function in the MC-eradicated mice. We sorted live (Vybrant$^+$) mature cardiac MCs (c–Kit$^+$FcεRI$^+$) at day 6 after MI, which expressed both connective tissue MC markers chymase (mMCP4) and tryptase (mMCP6; compared with nondetectable expression in cells sorted from the intestine; not depicted). Cardiac sorted MCs were transfected with tryptase siRNA or scramble siRNA (Fig. 8 H) for 16 h; viable cells were counted and were injected transcutaneously under echo-guidance into the myocardium of Cpa3$^{cre/+}$ mice at day 6 after infarction, 1 d before their physiological peak in the heart. Reconstitution of cardiac MCs transfected with scramble siRNA restored SF% of Cpa3$^{cre/+}$ mice as assessed at day 14 after infarction (WT: 28.15 ± 1.7% SF, Cpa3$^{cre/+}$: 18.5 ± 2.08% SF, Cpa3$^{cre/+}$ receiving MCs transfected with scramble SiRNA: 26.82 ± 2.9% SF; Fig. 8 I). However, injections with MCs transfected with MC tryptase siRNA failed to restored SF% of Cpa3$^{cre/+}$ (Fig. 8 I).

DISCUSSION

Here we report a novel role for cardiac MCs in the regulation of the myofilament force–Ca^{2+} relationship. Mature cardiac MCs respond functionally to MI and regulate myofilament cTnI and MyBPC phosphorylation. This integral MC-dependent effect preserves the contractile reserve in concert with Ca^{2+} flux to the sarcomeres (Arteaga et al., 2005; Solaro and Arteaga, 2007).

Mutations in c-Kit, as well as MC stabilization, have served as standard models to decipher MC functions. However, studies using c-kit mutations do not provide an exclusive functional role of MCs. As a prototypic example, kit mutant animals are protective against antibody–induced arthritis in contrast to Cpa3$^{cre/+}$ mice that are susceptible, proving that c-kit effects are not MC exclusive. Similarly, MC deficiency, in the absence of c-kit mutations, plays neither a role in the regulation of weight gain or insulin resistance (Gutierrez et al., 2015) nor in wound healing and skin carcinogenesis (Antsiferova et al., 2013). Similarly, the selectivity and the efficacy of using an MC stabilizer treatment, such as DSCG, have been questioned. DSCG failed to inhibit IgE-dependent MC degranulation in mice, and it had nonspecific inhibitory

effects on LPS-induced TNF release (Oka et al., 2012). In addition, several studies have identified MC-independent effects of DSCG treatment, including regulation of heat shock protein 90 (Okada et al., 2003), S100 proteins (Okada et al., 2002; Arumugam et al., 2006), and G protein–coupled receptor activation (Yang et al., 2010).

Hence, in an attempt to reevaluate the role of cardiac MCs, we assessed the functional effect of MC deficiency (Cpa3$^{cre/+}$ mice), c-kit deficiency (c-kitW/Wv mice), and inhibition of degranulation (DSCG administration) on cardiac function after infarction. In agreement with previous studies, we found increased MC density in the cardiac tissue after MI (Frangogiannis et al., 1998; Reid et al., 2011). Nevertheless, we show that, independently of c-Kit signaling, MCs preserve heart function via a mechanism that does not involve changes in cardiac remodeling after MI. Furthermore, we analyzed the recruitment of inflammatory cells and release of their mediators in the Cpa3$^{cre/+}$ mice. Our data showed no effects of MCs deficiency in the regulation of local inflammation at the times studied. However, besides the absence of MCs, a reduced basophil compartment has previously been observed in Cpa3$^{cre/+}$ animals, and this decrease should be considered when immunological functions are assessed in this model (Feyerabend et al., 2011).

Depressed cardiac function in response to MC deficiency is mediated by a reduction in cardiomyocyte cell shortening, the kinetics of contraction/relaxation, and Ca^{2+} sensitization, as reflected by a right shift on the Ca^{2+}–force response curve and an increase in EC$_{50}$. These effects correlated both with an increase in p-Ser22/23 cTnI, p-Ser273, and p-Ser282 MyBPC and increased PKA activity. Phosphorylation of cTnI at its N-terminal Ser22/23 residues leads to its dissociation (Finley et al., 1999) or low-affinity binding (Ward et al., 2003) to the N-terminal domain of cTnC (NTnC), blocking the transfer of the Ca^{2+} signal through NTnC to cTnI, then to actin and further along the thin filament (Sykes, 2003; Li et al., 2004). This PKA-dependent mechanism leads to decreased Ca^{2+} sensitivity (Ramirez-Correa et al., 2010), increased cross-bridge cycling, and accelerated relaxation of the muscle (Herron et al., 2001). In agreement with our findings, such posttranslational modifications on cTnI have been previously described in postinfarcted stunned myocardium and heart failure (Dong et al., 2012; Nixon et al., 2014; Thoemmes et al., 2014). PKA also phosphorylates Ser273, Ser282, and Ser302 of the N terminus of MyBPC, the region that binds to the S2 segment of myosin, close to its arm domain (Gruen et al., 1999). PKA-induced phosphorylation of MyBPC loosens the thick filament structure,

remodeling parameters in c-Kit W/Wv and DSCG-treated mice at day 14 after infarction, showing significantly increased levels of fibrosis in DSCG-treated mice and increased number of apoptotic cells in c-Kit W/Wv mice and DSCG-treated mice, with no effect on other parameters (n = 6). (D) Representative images of fibrosis, capillary density, infarct size, and apoptotic cardiac cells. Arrows point to representative apoptotic cells. All data represent two independent experiments. *, P < 0.05; **, P < 0.01; ***, P < 0.001, Mann–Whitney nonparametric test. All values are presented as mean ± SEM. PBS, PBS-treated animals; WT, Cpa3$^{+/+}$ littermates.
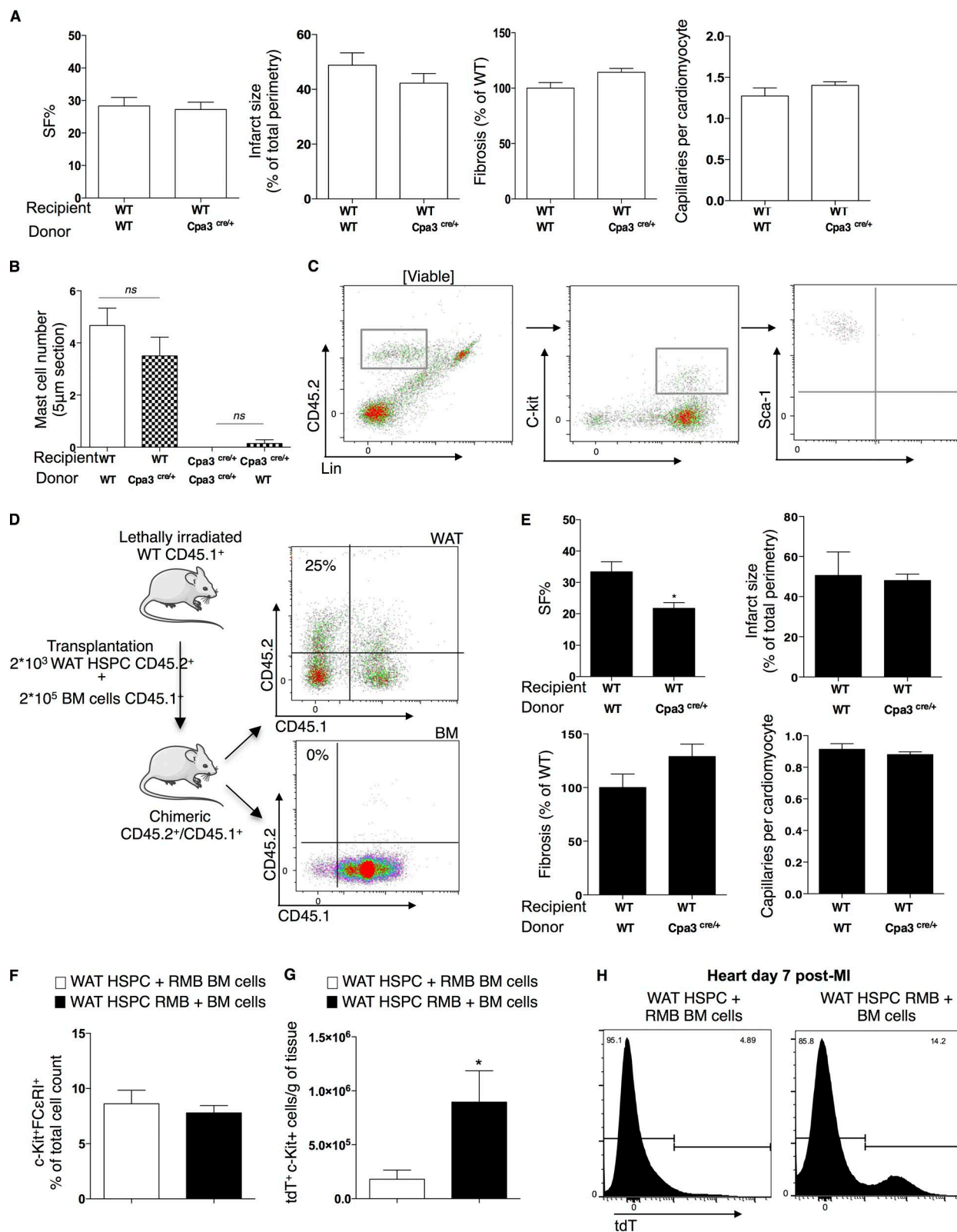
Figure 6.   **Cardiac MCs derive primarily from WAT HSPCs.** (A) Transplantation of WT mice with Cpa3[cre/+]-derived BM cells had no effect on left ventricular SF%, infarct size, fibrosis, and capillary density in reference to WT animals receiving WT-derived BM cells (*n* = 16, from three independent experiments). (B) Transplantation of lethally irradiated WT or Cpa3[cre/+] mice with WT or Cpa3[cre/+]-derived BM cells showed no reconstitution or inhibition of cardiac MCs,

preventing its binding to myosin, thereby changing force–Ca^{+2} response (Levine et al., 2001; Kulikovskaya et al., 2003) and altering contractile function (Stelzer et al., 2007). MyBPC phosphorylation is necessary for basal myocardial function, and both cardiac MyBPC-null mouse hearts and fully phosphorylated MyBPC show accelerated myofilament kinetics (Barefield and Sadayappan, 2010). Although increased PKA activity generally correlates with positive inotropic effects via L-type Ca^{+2} channel and phospholamban (PLB) phosphorylation, we saw no difference in Ca^{+2} transients, but rather a reduction in contractility via desensitization. The mechanisms by which such modulation of PKA is strictly affecting myofilament proteins and not calcium handling proteins are not clear. Specificity and efficiency of PKA substrate phosphorylation require spatial-temporal regulation of cAMP/PKA by A kinase–anchoring proteins (AKAPs). The latter possess the ability to coordinate signaling pathways by scaffolding different proteins and facilitating a unique PKA-regulated signal transduction (Manni et al., 2008). Possible changes that disrupt AKAP/PKA complexes with PLB or L-type Ca^{+2} channel or that regulate AKAPs docking PKA in proximity of its sarcomeric substrates (Rababa'h et al., 2015), such as the recently identified cardiac troponin C (Sumandea et al., 2011), could be possible mechanisms involved in the MC-dependent Ca^{+2} desensitization. Extensive further investigation will be needed to fully uncover how MCs regulate the contractile machinery in a PKA-dependent mechanism. Nevertheless, this is the first time that an MC to myofilament signal exchange is documented.

To further elucidate the mechanism of MC-dependent PKA inactivation, we sought to identify how MC signaling interferes with intracellular cardiomyocyte PKA. The PAR2 receptor is known to be cleaved/activated by MC-derived tryptases, and such cross-talk has already been identified between MCs and fibroblasts (McLarty et al., 2011; Murray et al., 2012). Indeed, MC tryptase was able to cleave PAR2 in vitro at the canonical site. Functionally, treatment of H9C2 cells with tryptase inhibited IBMX-induced PKA activation, and this effect was reproduced by treatment with the PAR2-AP, which is known to lead to Gi activation. Tryptase-induced PAR2 activation has been previously suggested to be pertussis toxin sensitive in airway smooth muscle cells

(Berger et al., 2001). Although PAR2 deficiency has been shown to be protective against infarct size and cardiac remodeling (Antoniak et al., 2010), studies with PAR2-AP in WT mice showed that PAR-2 mediates protective effects in cardiac ischemia/reperfusion injury (Napoli et al., 2000; McLean et al., 2002; Jiang et al., 2007; Zhong and Wang, 2009). Such difference in the functional outcome between PAR2-deficient mice and PAR2-AP rely on the fact that the activating peptide changes the receptor's three-dimensional structure and subsequently its "biased agonism" in ways that cannot be compared with its activation by proteases such as tryptase (Rajagopal et al., 2010). In agreement with our findings, however, Somasundaram et al. (2005) identified PAR2-AP mimicking the signaling transduction of tryptase in canine venous endothelial cells after ischemia/reperfusion, and others have shown the same effects in a variety of pathological models (Corvera et al., 1997; Akers et al., 2000; Berger et al., 2001; Shpacovitch et al., 2002). In conclusion, our data propose a novel function of tryptase-induced PAR2 activation, similar to that of PAR2-AP, which regulates the intracellular PKA activity of cardiomyocytes.

MC trafficking in response to inflammatory or allergic triggers has been mainly attributed to BM-derived MCPs that circulate in the blood and home peripheral tissues before reaching terminally differentiated mature MCs. WAT has been described to contain stem cells with multilineage properties (Cousin et al., 2003; Han et al., 2010; Poglio et al., 2010, 2012) that may be of clinical value in repair or replacement of various cell lineages (Tran and Kahn, 2010). Recent studies have described both MCs (Liu et al., 2009) and MCPs (Poglio et al., 2010) in WAT. Poglio et al. (2010) documented that the WAT stromal vascular fraction hosts an MC lineage that does not originate from the BM and that can home to peripheral tissues including the skin and the intestine. MCs of WAT origin are infiltrating the cardiac tissue more efficiently than the BM competitor cells. Similarly, in chimeric mice whose BM cells were donated from GFP transgenic animals, cardiac MCs populating the ischemic milieu did not carry the GFP transgene, suggesting that MCs that home to the infarcted heart do not arise from BM progenitors (Fazel et al., 2006). Nevertheless, the density of MCPs was increased in the BM, and a small proportion of the mature cardiac MCs after MI did originate

respectively, as counted on TB-stained heart sections ($n = 6$–12, two independent experiments). Kruskal–Wallis and Dunn's post hoc test for comparisons between groups. (C) Representative flow cytometry gating strategy for isolation of HSPCs (CD45.2$^+$c-kit$^+$Sca-1$^+$) in WAT showing the lack of mature FcɛRI$^+$ MCs. (D, left) Schematic overview of co-transplantation of lethally irradiated CD45.1$^+$ WT mice with both FACS-sorted WAT-HSPCs (c-kit$^+$Lin$^-$Sca$^+$) from CD45.2$^+$ mice and BM cells from CD45.1$^+$ cells. WAT-HSPCs were isolated from WT, Cpa3$^{cre/+}$, or RMB mice. (right) Representative example of chimerism evaluation in the WAT and the BM by flow cytometry–assisted counting of WAT-derived CD45.2$^+$ cells in CD45.1$^+$ recipient mice transplanted with both FACS-sorted WAT-HSPCs from WT CD45.2$^+$ mice and BM cells from WT CD45.1$^+$ cells. (E) Transplantation of WT mice with WAT-HSPCs from Cpa3$^{cre/+}$ led to depressed left ventricular SF% at day 14 after infarction ($n = 7$, two independent experiments) without any changes in infarct size, fibrosis, and capillary density. *, $P < 0.05$, Mann–Whitney nonparametric test. (F) WT mice transplanted with either WAT-HSPCs and RMB-derived BM cells or RMB-derived WAT HSPCs and BM cells have equal amounts of mature cardiac MCs at day 7 after infarction ($n = 4$–5, two independent experiments). (G) Cardiac tdT$^+$c-kit$^+$ cell numbers were higher in the WT mice transplanted with RMB-derived WAT HSPCs and BM cells compared with those transplanted with WAT-HSPC and RMB-derived BM cells (day 7 after MI; $n = 8$–10, two independent experiments). *, $P < 0.05$, Mann–Whitney nonparametric test. (H) Representative image of tdT$^+$ cells in the heart 7 d after infarction. All values are presented as mean ± SEM. ns, not significant; WT, Cpa$^{+/+}$ littermates.
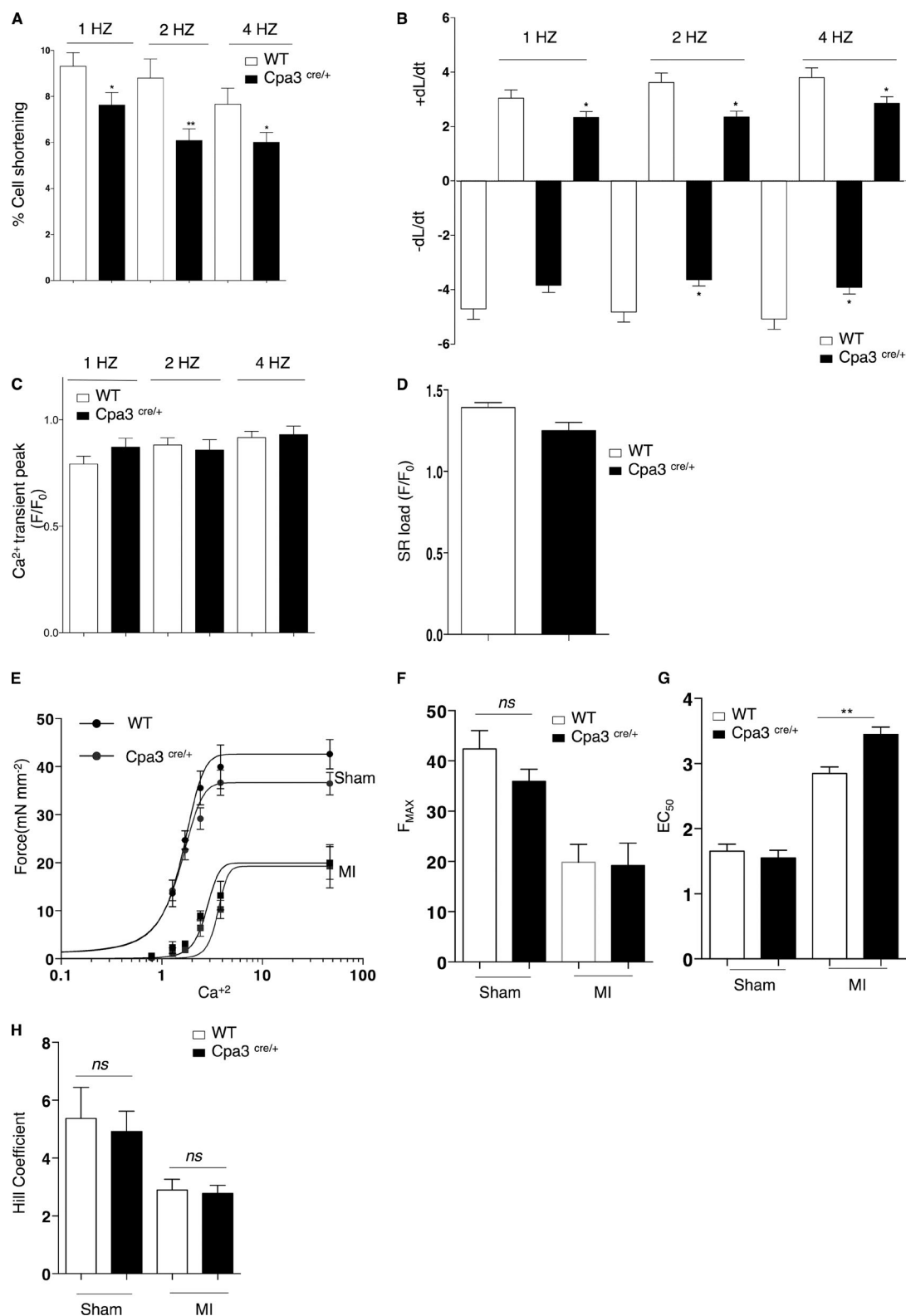
Figure 7.   **Reduced contractility and myofilament Ca²⁺ sensitization in Cpa3^cre/+ mice after infarction.** (A) Depressed left ventricular cardiomyocyte cell shortening (%) of Cpa3^cre/+-derived intact cardiomyocytes versus WT cardiomyocytes in response to field stimulation (1, 2, and 4 Hz; n = 30–50, two independent experiments). *, P < 0.05; **, P < 0.01, Kruskal–Wallis and Dunn's post hoc test for comparisons between groups. (B) Both contraction and relaxation kinetics were significantly reduced in Cpa3^cre/+-derived cardiomyocytes versus WT cardiomyocytes (n = 30–50, two independent experiments).

from the BM progenitors. Therefore, although we cannot exclude the BM as a source of cardiac MCs, MCPs originating primarily from the WAT dominate in the infarcted heart in our experimental conditions. Interestingly, in metabolic disorders and obesity, MC density in WAT is increased, suggesting a defect in their homing and/or production. Further studies are required to understand how homing of WAT MCs is regulated in response to acute MI or other related morbidities such as diabetes and obesity (Liu et al., 2009; Divoux et al., 2012) and would be of great therapeutic interest.

We identified a novel role for cardiac MCs in preserving postischemic cardiac function. In response to MI, WAT-derived MCPs are mainly recruited to the cardiac tissue, proliferate, and differentiate into mature cells in an SCF-dependent manner. MC deficiency reduces PKA-mediated myofilament phosphorylation and Ca^{2+} sensitization (Fig. 9). In conclusion, MCs can directly regulate the contractile machinery of cardiomyocytes, and their presence in the infarcted myocardium is indispensable. Identification of the mechanisms that regulate MC activation and its signaling on PKA-dependent sarcomere function will provide novel insights in the regulation of contractile function after acute MI.

MATERIALS AND METHODS

MI. All experiments were conducted according to the ethical committee for animal experimentation (Paris Descartes University, CEEA 34) and the National Charter on the ethics on animal experimentation from the French Minister of High Education and Research under the following reference: Molecular and cellular mechanisms involved in post-ischemic tissue remodelling (project n° 13-06/reference MESR: n° 01373.01).

C57BL/6J mice were obtained from Janvier (backcrossed at least 12 times). MC-sufficient WBB6F1/J-Kit$^{+/+}$ and MC-deficient WBB6F1/J-KitW/KitWv/J mice were obtained from The Jackson Laboratory (backcrossed at least 10 times). C57BL/6J mMCP4$^{-/-}$ and their WT littermates (mMCP4$^{+/+}$, WT) mice were provided by U. Blank (backcrossed at least seven times). C57BL/6J Cpa3$^{cre/+}$ mice and their WT littermates (Cpa3$^{+/+}$, WT) were a gift from H.-R. Rodewald (backcrossed at least eight times). All mice were studied at the age of 8 wk. MI was induced by left coronary ligation as previously described (Kumar et al., 2005). Mice were anesthetized using ketamine (100 mg/kg body weight)

and xylazine (10 mg/kg body weight) via intraperitoneal injection, intubated, and ventilated using a small-animal respirator. The chest wall was shaved, and a thoracotomy was performed in the fourth left intercostal space. The pericardial sac was removed, and the left anterior descending artery was permanently ligated using a 7/0 monofilament suture (Peters Surgical) at the site of its emergence close to the left atrium. The thoracotomy was closed with 6/0 monofilament sutures. The exact same procedure was performed for the sham-operated mice except that the ligation was not tied. The endotracheal tube was removed once spontaneous respiration resumed, and mice were placed on a warm pad at 37°C until awakened. For the DSCG treatment experiments, mice were treated with DSCG (50 µg/g/mouse) or PBS (150 µl) 1 h after the operation and every day for 7 d. For evaluation of SCF effect on MC proliferation and density, mice were treated with the anti-SCF antibody provided by N.W. Lukacs and S. Morris (Medical School, University of Michigan, Ann Arbor, MI; Dolgachev et al., 2009) or rabbit serum (400 µl/mouse; Sigma-Aldrich) at days 1, 3, and 5 after infarction. For assessment of cell proliferation with the APC BrdU Flow kit (BD), 100 µl BrdU was intraperitoneally injected into mice 24 h before tissue isolation and digestion.

BM and WAT transplantation. BM cells were flushed from the femurs of C57BL/6J under sterile conditions, and 8×10^6 cells were injected into the retroorbital sinuses of C57BL/6J mice irradiated with 10 Gy (one dose). Competitive repopulation assays were conducted as described previously (Poglio et al., 2010, 2012). In brief, 2×10^3 c-Kit$^+$/Lin$^-$/Sca-1$^+$ cells sorted from the WAT of donor mice were mixed with 2×10^5 competitor BM total cells. The mixed population was intravenously injected into lethally irradiated (10 Gy, 137Cs source) recipient mice. Reconstituted mice were then allowed to recover for 2 mo before MI.

Echocardiographic measurements. Transthoracic echocardiography was performed 14 d after surgery using an echocardiograph (ACUSON S3000 ultrasound; Siemens AG) equipped with a 14-MHz linear transducer (1415SP). The investigator was blinded to group assignment. Mice were anesthetized by isofluorane inhalation. Percentages of SF (%SF; Zouggari et al., 2013) or EF (%EF) were calculated as previously described (Dormishian et al., 2013).

---

*, $P < 0.05$, Kruskal–Wallis and Dunn's post hoc test for comparisons between groups. (C) MC deficiency had no effect on Ca^{2+} transient peak ($n = 30$–50, two independent experiments). (D) SR Ca^{2+} content in response to 1-Hz electric stimulation and after caffeine (10 mmol/l) was similar in both WT and Cpa3$^{cre/+}$-derived cardiomyocytes ($n = 30$–50, two independent experiments). (E) Force–calcium fitted curves reflecting Ca^{2+} responsiveness of left ventricle peri-infarcted skinned myocytes from WT and Cpa3$^{cre/+}$ mice after sham operation or MI. Reduced Ca^{2+} sensitivity in both WT and Cpa3$^{cre/+}$-derived skinned myocytes in response to MI with a shift to the right in Cpa3$^{cre/+}$-derived myocytes versus WT ($n = 5$–8, two independent experiments). (F and G) F_{max} was not altered between WT and Cpa3$^{cre/+}$-derived myocytes (F), but MC deficiency caused Ca^{2+} desensitization with a significant increase in EC_{50} (G; $n = 5$–8, two independent experiments). **, $P < 0.01$, Kruskal–Wallis and Dunn's post hoc test for comparisons between groups. (H) No difference in Hill coefficient as a measure of Ca^{2+} cooperativity ($n = 5$–8, two independent experiments). All values are presented as mean ± SEM. ns, not significant; Sham, sham-operated animals; SR, sarcoplasmic reticulum.
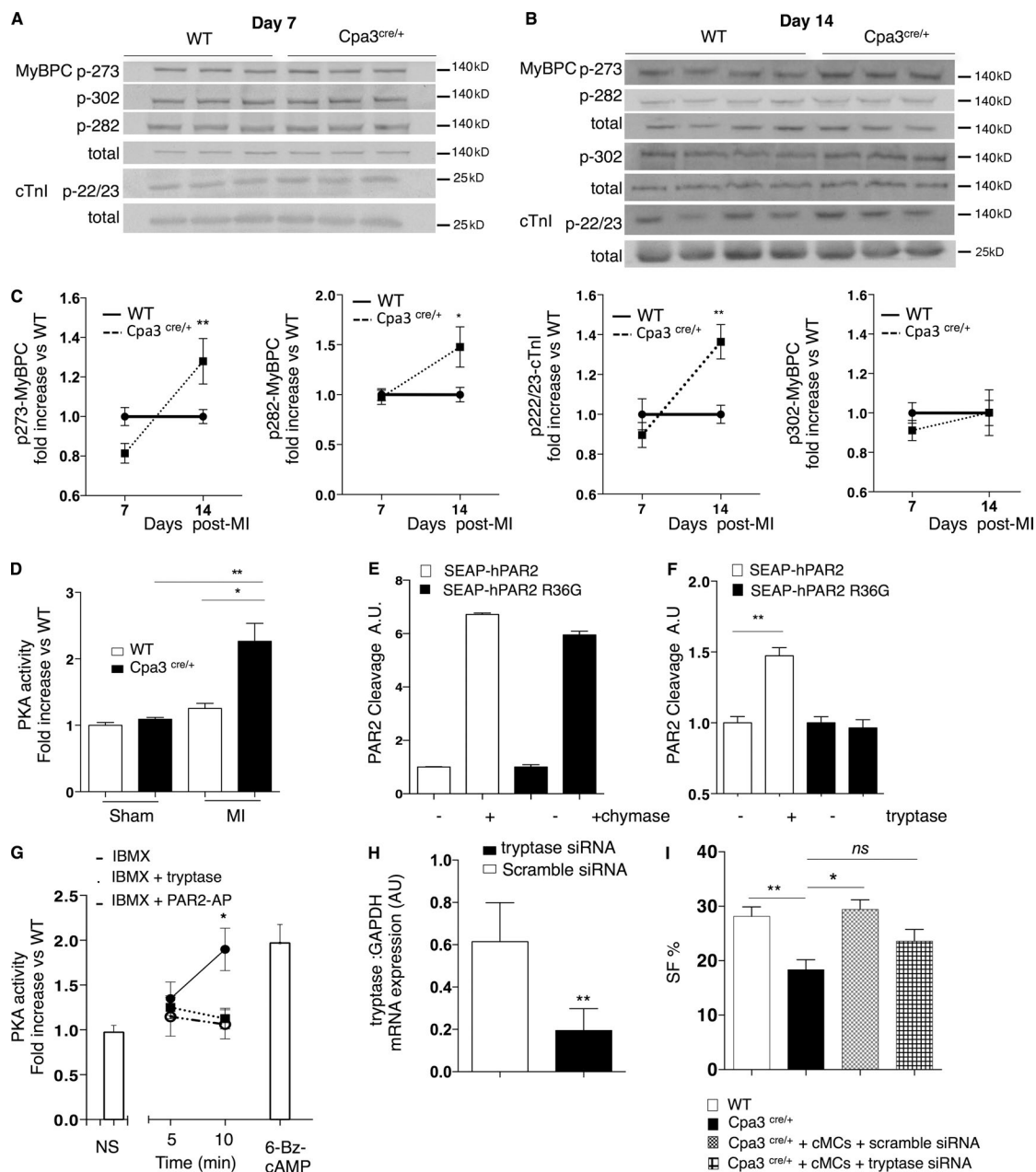
1366

The role of mast cells in myocardial infarction | Ngkelo et al.

Figure 8. **MC–dependent myofilament phosphorylation via tryptase–induced PAR2 activation.** (A and B) Representative Western blots for phosphorylated cTnI (Ser22/23) and MyBPC (Ser273, Ser302, and Ser282) and total proteins levels from peri-infarcted cardiac tissue of WT and Cpa3[cre/+] at day 7 after MI (A) and at day 14 after infarction (B). (C) Quantified levels of p273-, p282-, and p302-MyBPC and p22/23-cTnI normalized to total protein levels showing increased myofilament phosphorylation in Cpa3[cre/+] mice at day 14 after infarction ($n = 7$–13, three independent experiments). *, $P < 0.05$; **, $P < 0.01$, Kruskal–Wallis and Dunn's post hoc test for comparisons between groups. (D) Increased PKA activity (A.U.) in peri-infarcted area of Cpa3[cre/+] cardiac tissue at day 14 after infarction ($n = 4$ for sham, $n = 10$ for MI from four independent experiments). *, $P < 0.05$; **, $P < 0.01$, Kruskal–Wallis and Dunn's post hoc test for comparisons between groups. (E) Treatment with recombinant MC chymase cleaved PAR2 in a non–R36-specific/canonical manner ($n = 3$, two independent experiments). (F) Recombinant mouse tryptase cleaved PAR2 only at canonical R36 site ($n = 4$, two independent experiments). **, $P < 0.01$, Kruskal–Wallis and Dunn's post hoc test for comparisons between groups. (G) IBMX-induced activation of PKA in H9C2 cardiomyocytes is inhibited in the presence of tryptase or PAR2-AP; 6-Bz-cAMP was used as a positive control ($n = 4$, two independent experiments). *, $P < 0.05$, Kruskal–Wallis and Dunn's post hoc test for comparisons between groups. (H) siRNA-induced mRNA knockdown of tryptase in cardiac MCs at 16 h after transfection ($n = 4$, two independent experiments). **, $P < 0.01$, Mann–Whitney nonparametric test. (I) Depressed SF% (day 14) is restored in Cpa3[cre/+] mice by trans-cutaneous (echo-guided) injection of cardiac FACS-sorted Vybrant[+] MCs (sorted at day 6 after infarction; $n = 7$) but not restored by MCs treated with tryptase siRNA ($n = 3$). All data are from two independent experiments. *, $P < 0.05$; **, $P < 0.01$, Kruskal–Wallis and Dunn's post hoc test for comparisons between groups. All values are presented as mean ± SEM. ns, not significant.
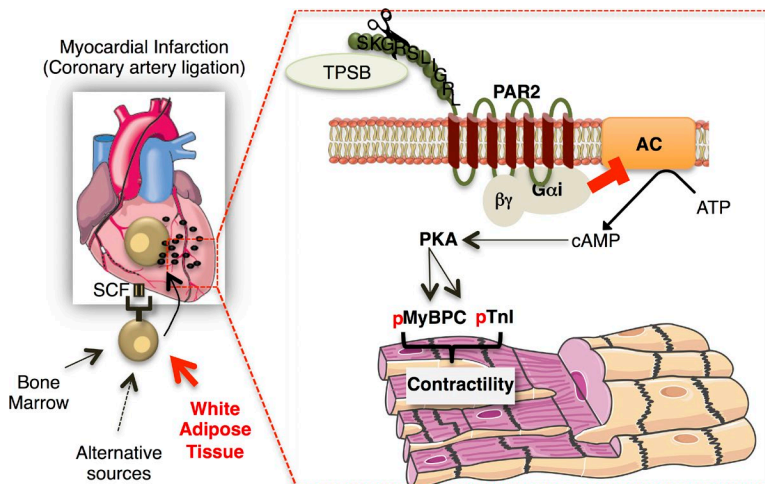
Figure 9. **Schematic diagram showing the proposed mechanism of MC–dependent myofilament Ca²⁺ sensitization after MI.** MCs, originating primarily from WAT, infiltrate the heart after MI and regulate cardiac function via regulation of myofilament protein phosphorylation, cTnI, and MyBPC. The mechanism proposed involves tryptase-regulated PAR2 activation with subsequent Gi activation inhibiting cAMP/PKA activity. AC, adenylyl cyclase; p, phosphoryl group.

Immunohistochemistry. Cardiac remodeling after MI was assessed at day 14. Hearts were excised, rinsed in PBS, and frozen in liquid nitrogen. Hearts were cut by a cryostat (CM 3050S; Leica) into 5–7-μm-thick sections. TB was used to assess MC degranulation as previously described (Xaubet et al., 1991). Masson's trichrome and Sirius red stains were performed for infarct size and myocardial fibrosis evaluation. Infarct size (in %) was calculated as total infarct circumference divided by total left ventricle circumference. The collagen volume fraction was calculated as the ratio of the total area of interstitial fibrosis to the myocytes area in the entire visual field of the section. Endothelial cells within capillaries were visualized after BS-1 lectin staining (1:100, FITC-conjugated Griffonia simplicifolia; Sigma-Aldrich) and cardiomyocytes with wheat germ agglutinin (1:200, Texas red conjugated; Thermo Fisher Scientific). Image analysis and measurements were conducted with ImageJ processing program (National Institutes of Health).

Cleavage assay for PAR2 receptor. Secreted epithelial alkaline phosphatase (SEAP)–tagged versions of human PAR2 (UniProtKB accession P55085; fused at Q27) protein as well as the canonical cleavage site mutant R36G were generated to allow quantification of receptor cleavage (Ludeman et al., 2004). PAR1 (F2r) knockout mouse lung fibroblasts (KOLFs; Trejo et al., 1996) were grown in DMEM supplemented with antibiotics and 5% serum. Transfection was performed with TransitLT1 transfection (Euromedex) in complete medium as recommended. 48 h after transfection, cells were washed with Opti-MEM for 1 h and incubated for one additional hour in Opti-MEM with or without the respective MC-specific proteases (500 ng/ml), and supernatants were collected. A second 20-min incubation with 10 nM trypsin stripped all remaining SEAP moiety (as verified in separate experiments) from the cell surface. SEAP activity in the conditioned media was determined at OD405 after hydrolysis of para-nitrophenyl phosphate (pNPP; Sigma-Aldrich). This permitted calculation of percentage of surface receptors cleaved during the initial 60-min incubation.

Membrane–permeabilized myocytes. Membrane-permeabilized or "skinned" myocyte experiments were performed as previously described (Kirk et al., 2014). Tissue from the peri-infarct zone was flash frozen in liquid nitrogen and stored at −80°C. At the time of the experiment, the tissue was homogenized in isolation solution (5.5 mM Na₂ATP, 7.11 mM MgCl₂, 2.0 mM EGTA, 108.01 mM KCl, 8.91 mM KOH, 10 mM imidazole, 10 mM DTT, protease inhibitors [Sigma-Aldrich], and phosphatase inhibitors [Roche] with 0.3% Triton X-100). Triton X-100 is a detergent that permeabilizes the myocyte membrane, allowing the free movement of calcium into the cell. Myocytes were then washed in isolation solution without Triton X-100 to remove the detergent. Using silicone, a single myocyte was glued to the tips of 150-μm diameter minutia pins. One pin was attached to a force transducer (Aurora Scientific Inc.). A video camera (Imperx) and the high-speed video sarcomere length program (Aurora Scientific Inc.) were used to continuously monitor sarcomere length. Studies were conducted at a sarcomere length of 2.0 μm. The mounted myocytes were kept in a relax buffer (5.95 mM Na₂ATP, 6.41 mM MgCl₂, 10 mM EGTA, 100 mM BES, 10 mM phosphocreatine, 50.25 mM potassium propionate, 10 mM DTT, and protease and phosphatase inhibitors) with no calcium. Force was measured as the myocyte was exposed to increasing calcium concentrations, by moving the myocyte from baths containing different ratios of relax and activating solutions. The activating solution contained 5.95 mM Na₂ATP, 6.2 mM MgCl₂, 10 mM Ca²⁺EGTA, 100 mM BES, 10 mM phosphocreatine, 29.98 mM potassium propionate, 10 mM DTT, and protease and phosphatase inhibitors. All buffers were adjusted to a pH of 7.0. A complete activation of the myocyte occurred at the beginning and end of the experiment, and the myocyte was discarded if there was <10% rundown. Force–calcium data were fit to the Hill equation: $F = F_{max} \times C_a^h / (EC_{50}^h + Ca^h)$, yielding F_{max}, calcium sensitivity (Ca²⁺ required to achieve 50% maximal force, EC_{50}), and cooperativity (Hill coefficient, h).

Organ digestion/cell isolation. Peripheral blood was isolated from the inferior vena cava puncture with heparin solution. Whole blood was lysed after immunofluorescence staining using the FACS lysing solution (BD), and total blood leukocyte numbers were counted using trypan blue (Sigma-Aldrich). BM cells were washed through the femur and the tibia and filtered through a 40-μm nylon mesh (BD). Spleens were collected, minced with fine scissors, and filtered through a 40-μm nylon mesh (BD). For both splenocytes and BM-erived cells, the cell suspension was centrifuged at 400 g for 10 min at 4°C. Red blood cells were lysed using red blood cell lysing buffer (Sigma-Aldrich), and splenocytes and BM cells were washed with PBS supplemented with 1% vol/vol fetal bovine serum. Hearts were collected, and the left ventricle was isolated, minced with fine scissors, and gently passed through the Bel-Art Scienceware 12-well tissue disaggregator (Thermo Fisher Scientific). Cells were collected, filtered through 40-μm nylon mesh, and washed with PBS with 1% vol/vol fetal bovine serum. Subcutaneous WAT was dissected and mechanically dissociated. WAT fragments were digested with collagenase, and stroma-vascular cells were collected by centrifugation after elimination of undigested fragments by filtration as described previously (Poglio et al., 2010). Red blood cells were removed by incubation in hemolysis buffer (STEMCELL Technologies). Cells were counted and used for HSPC sorting.

Flow cytometry. Cells isolated from the tissue of interest were incubated in the dark at 4°C for 30 min with the following antibody mix. For mature MCs: APC-conjugated ckit/CD117 (2B8; BD) and PE-Cy7–conjugated Ly-6A/E (Sca-1; D7; BD). For MCPs: DAPI-conjugated Lineage (eBioscience), FITC-conjugated CD45.2 (BD), CD45.1 (BD), APC-conjugated CD34 (HM34; BioLegend), PerCP/Cy5.5-conjugated CD16/32 (FcγII/III; Thermo Fisher Scientific), and PE-conjugated Integrin-β7 (FIB504; eBioscience). When cardiac-derived cells were analyzed for marker expression, Vybrant DyeCycle violet stain (Thermo Fisher Scientific) was used to stain live cells and eliminate both debris subsequently nonspecific autofluorescence. For detection of cardiac MCs, granulated cells were first gated on SSC/FSC. The total number of cells was normalized to tissue weight. Cells were analyzed using a flow cytometer (LSR II; BD) or were sorted with FACSAria II (BD). The APC BrdU Flow kit (BD) was used for analysis of proliferation according to the manufacturer's instructions. HSPC isolation was performed as previously described (Poglio et al., 2010). In brief, freshly isolated WAT–stromal vascular fraction (SVF) cells were stained in PBS containing FcR Block reagent and CD117 (2B8; BD), Lineage (BD), Sca-1 (E13-161.7; BD), and CD45.2 (BD) antibodies. Cells were washed in PBS and sorted with FACSAria II. Data acquisition and analysis were performed using FACSDiva software (BD) or FlowJo 7.5.

For detection of inflammatory cells, total cardiac cells were gated on PerCP-conjugated CD45 (BD), and the following antibodies were used: DAPI-conjugated anti-CD11b (BD), PE-conjugated anti-Ly6G (1A8; BD), APC-conjugated anti-F4/80 (BioLegend), FITC-conjugated anti-Ly6C (BioLegend), APC-conjugated anti-CD8a (BD), PE-conjugated anti-CD45R/B220 (RA3-6B2; eBioscience), PE–Alexa Fluor 700–conjugated anti-CD3 (eBioscience), and FITC-conjugated anti-CD4 (eBioscience). All antibodies were used at a dilution of 1:100. Monocytes were identified as CD11b^{hi}Ly6G$^-$7/4$^{hi/lo}$. Neutrophils were identified as CD11b$^+$Ly6G^{hi}. Macrophages were identified as CD11b$^+$Ly6G$^-$F4/80$^+$. Mature B lymphocytes were identified as B220$^+$CD3$^-$ and T cells as CD4$^+$CD3$^+$ or CD4$^+$CD8$^+$. The total number of cells was then normalized to heart weight. Cells were analyzed using a flow cytometer (LSR II).

Transcutaneous echo–guided intramyocardial injections of cardiac MCs. For each experiment, cardiac MCs were FACS sorted as Vybrant$^+$c-kit$^+$FcεRI$^+$ cells from a total of 30 C57BL/6J mice at day 6 of MI. Hearts were collected, and the left ventricle was isolated, minced with fine scissors, and gently passed through the Bel-Art Scienceware 12-well tissue disaggregator (Thermo Fisher Scientific). Cells were then collected and filtered through 40-μm nylon mesh. During sorting, cells were kept always in PBS complemented with 5% fetal calf serum at 4°C under sterile conditions. FACS-sorted MCs were counted, plated at a density of 2.5×10^5 cells/ml, and cultured in DMEM complemented with 20 mM L-glutamine, 10% fetal calf serum (inactivated at 56°C), 2 mM L-glutamine, 1 mM pyruvate, 100 U/ml penicillin/streptomycin, and 1% MEM nonessential amino acid solution (Sigma-Aldrich) in the presence of 0.1 mg/ml recombinant mouse SCF for MC survival overnight. Cells were then transfected with the Nucleofector 2B device (program C-005) in 100 μl Nucleofector solution T (Lonza) with ON-TARGETplus Mouse Tpsb2 (mMCP6) siRNA (L-064669-02-0005; GE Healthcare) or non-targeting (scramble) siRNA (GE Healthcare) for 16 h according to the manufacturer's instructions. Cells were washed, their viability was assessed with Trypan blue, and they were counted and resuspended in PBS to give a total of 80,000 cells/60 μl of suspension for trans-cutaneous injections. Closed-chest, trans-cutaneous, echo-guided injections were then used to deliver cells or PBS directly to the peri–infarcted myocardium as previously described (Toeg et al., 2013). In brief, Cpa3$^{cre/+}$ mice with 6-d-old infarcts were anesthetized by isoflurane inhalation and fixed in a supine position on a heating pad. The infarct region was located by echocardiography using a Vevo 2100 imaging system and a MS400 probe appropriate for mouse cardiovascular imaging (18–38 MHz; VisualSonics Inc.). A micromanipulator (VisualSonics) was used to guide a 1.5-in-long 27-G needle (Dominic Dutscher) into the hypokinetic anterior wall of the peri–infarcted myocardium under continual echo guidance. Four 15-μl injections were used to deliver a total of 80,000 cells resuspended in sterile PBS.

FlowCytomix. The bead-based multiplex immunoassay for the flow cytometer (eBioscience) was used to measure the levels of inflammatory mediators in the cardiac tissue. Peri-infarcted left ventricular tissue was homogenized using a glass Dounce homogenizer in ice-cold Tris-HCl (50 mmol/l, pH 7.5), NaCl (150 mmol/l), EDTA (1 mmol/l), NP-40 (1%), Na-orthovanadate (1 mM), β-glycerophosphate (40 mM; Sigma-Aldrich), and protease cocktail inhibitors (Roche). 500 µg protein homogenates was incubated with antibody-coated beads recognizing IL3, Mcp3, Mcp1, IL-6, IL-10, IL1β, IL12p70, and TNF. The target analytes were captured by the specific antibodies, and the samples were incubated with biotin-conjugated secondary antibodies. Streptavidin–PE was added for detection, and flow cytometry was used to differentiate bead populations according to size and fluorescent signature. Analyte concentration was measured using standard curves on the FlowCytomix Pro Software (eBioscience). Data were expressed as picogram of analyte per microgram of cardiac protein homogenate.

Quantitative real-time PCR. Quantitative real-time PCR was performed on a Step-One Plus (Applied Biosystems). GAPDH was used to normalize gene expression. The following primer sequences were used: SCF forward, 5′-GGAGATCTGGAA TCCTGTGA-3′; and reverse, 5′-CCCGGCGACATAGTT GAGGGTTAT-3′; mMCP6 forward, 5′-CTGGGGCGA CATTGATAATGACGAGCCTCT-3′; and reverse, 5′-CCC CCTGAATCGCCCTGGCAGGAGT-3′; and mMCP4 forward, 5′-CTGGGGCTGGAGCTGAGGAGATTA-3′; and reverse, 5′-CAACACAAATTGGCGGGTTATGAGAA-3′.

Tissue homogenization and Western blot. Cardiac tissue was homogenized using a glass Dounce homogenizer in ice-cold Tris-HCl (50 mmol/l, pH 7.5), NaCl (150 mmol/l), EDTA (1 mmol/l), NP-40 (1%), Na-orthovanadate (1 mM), β-glycerophosphate (40 mM; Sigma-Aldrich), and protease cocktail inhibitors (Roche). After homogenization, protein concentration was measured by the SMART Micro BCA Protein Assay kit (Intron). Total tissue homogenate was denatured in loading buffer and 0.1 M DTT at 95°C for 5 min, and 30 µg was loaded on freshly prepared 9% Bis-Acrylamide gels (ratio 29:1), transferred onto nitrocellulose membranes (Bio-Rad Laboratories), and blotted using custom MyBPC antibodies against phospho Ser-273 (1:2,500), Ser-282 (1:2,500), and Ser-302 (1:10,000) and total (1:5,000; Kirk et al., 2014); phospho TnI (1:1,000; Cell Signaling Technology); and total TnI (1:10,000; Spectral Diagnostics). In some cases, blots were stripped with freshly prepared stripping buffer (2 M Tris-HCL, pH 6.8, 10% SDS, and 100 mM β-mercaptoethanol) and reprobed. Blots were scanned before being reprobed to ensure efficient stripping. All phosphorylated protein levels were normalized to total protein levels.

Cardiomyocyte contractility and Ca^{2+}-transient measurements. Left ventricle myocytes were freshly isolated from the noninfarcted free wall and recorded as previously described (Fauconnier et al., 2010). Real-time Ca^{2+} measurements and cell shortening were performed on freshly isolated myocytes incubated in a physiological Tyrode solution (140 mM NaCl, 5 mM KCl, 8 mM NaH_2PO_4, 1 mM $MgSO_4$, 10 mM HEP ES, 5 mM Taurine, and 10 mM glucose). Cardiomyocytes were loaded with the ratiometric Ca^{2+} dye Fura-2AM at room temperature for 20 min (2 µM, Invitrogen), and cell shortening/Ca^{2+} transients were recorded using electrical-field stimulation (1, 2, and 4 Hz). Fluorescence wavelengths emitted at 340 nm (F340) and 380 nm (F380) were simultaneously recorded using the IonOptix system coupled to a microscope (×40; ZEISS). SR Ca^{2+} content was evaluated by measuring the peak amplitude of the cytosolic Ca^{2+} transient induced by rapid perfusion of caffeine (10 mM) after a 20-s pacing period (1 Hz) followed by a 10-s rest period with a calcium-sodium–free solution containing 140 mM LiCl, 6 mM KCl, 1 mM $MgCl$, 1 mM EGTA, 10 mM glucose, and 10 HEPES, pH 7.4.

Cell culture. H9c2 cells, derived from the embryonic rat ventricle (ATCC CRL1446), were seeded at a density of 5×10^5 cells/100-mm plate and cultured at 37°C in a 5% CO_2 humidified atmosphere in DMEM supplemented with 0.2 mM glutamine, 100 U/ml penicillin, 100 µg/ml streptomycin, and 10% FBS. When cells reached a subconfluence state (80%), they were treated with IBMX (3-isobutyl-1-methylxanthine; Sigma-Aldrich) at 100 µM for 5 and 10 min with or without co-treatment with 500 ng/ml mouse recombinant tryptase (R&D Systems) or the 100 µM PAR2-AP SLIGRL-NH₂ (Abcam). Cells were homogenized and sonicated in cell lysis buffer (#9803; Cell Signaling Technology), and protein concentration was measured by the SMART Micro BCA Protein Assay kit (Intron).

PKA activity assay. PKA activity was measured by the commercial kit (Enzo Life Sciences) according to manufacturer's instructions. In essence, active PKA was used to generate a standard curve, and 15 µg of cardiac peri-infarcted tissue homogenate or 10 µg of cell lysate was used for the assay.

Statistical analysis. Group comparisons were made using the Kruskal–Wallis test by ranks (nonparametric one-way analysis of variance), with Dunn's post hoc comparisons. Normal distribution was evaluated with the Shapiro–Wilk test. For individual comparisons, Mann–Whitney's U test was used as described in the figure legends. All values are presented as mean ± SEM, and a p-value <0.05 was considered significant.

REFERENCES

Akers, I.A., M. Parsons, M.R. Hill, M.D. Hollenberg, S. Sanjar, G.J. Laurent, and R.J. McAnulty. 2000. Mast cell tryptase stimulates human lung fibroblast proliferation via protease-activated receptor-2. *Am. J. Physiol. Lung Cell. Mol. Physiol.* 278:L193–L201.

Antoniak, S., M. Rojas, D. Spring, T.A. Bullard, E.D. Verrier, B.C. Blaxall, N. Mackman, and R. Pawlinski. 2010. Protease-activated receptor 2 deficiency reduces cardiac ischemia/reperfusion injury. *Arterioscler. Thromb. Vasc. Biol.* 30:2136–2142. http://dx.doi.org/10.1161/ATV BAHA.110.213280

Antsiferova, M., C. Martin, M. Huber, T.B. Feyerabend, A. Förster, K. Hartmann, H.R. Rodewald, D. Hohl, and S. Werner. 2013. Mast cells are dispensable for normal and activin-promoted wound healing and skin carcinogenesis. *J. Immunol.* 191:6147–6155. http://dx.doi.org/10.4049 /jimmunol.1301350

Arteaga, G.M., C.M. Warren, S. Milutinovic, A.F. Martin, and R.J. Solaro. 2005. Specific enhancement of sarcomeric response to Ca^{2+} protects murine myocardium against ischemia-reperfusion dysfunction. *Am. J. Physiol. Heart Circ. Physiol.* 289:H2183–H2192. http://dx.doi.org/10 .1152/ajpheart.00520.2005

Arumugam, T., V. Ramachandran, and C.D. Logsdon. 2006. Effect of cromolyn on S100P interactions with RAGE and pancreatic cancer growth and invasion in mouse models. *J. Natl. Cancer Inst.* 98:1806–1818. http://dx .doi.org/10.1093/jnci/djj498

Barefield, D., and S. Sadayappan. 2010. Phosphorylation and function of cardiac myosin binding protein-C in health and disease. *J. Mol. Cell. Cardiol.* 48:866–875. http://dx.doi.org/10.1016/j.yjmcc.2009.11.014

Berger, P., D.W. Perng, H. Thabrew, S.J. Compton, J.A. Cairns, A.R. McEuen, R. Marthan, J.M. Tunon De Lara, and A.F. Walls. 2001. Tryptase and agonists of PAR-2 induce the proliferation of human airway smooth muscle cells. *J. Appl. Physiol.* 91:1372–1379.

Boag, S.E., R. Das, E.V. Shmeleva, A. Bagnall, M. Egred, N. Howard, K. Bennaceur, A. Zaman, B. Keavney, and I. Spyridopoulos. 2015. T lymphocytes and fractalkine contribute to myocardial ischemia/ reperfusion injury in patients. *J. Clin. Invest.* 125:3063–3076. http://dx .doi.org/10.1172/JCI80055

Chen, C.C., M.A. Grimbaldeston, M. Tsai, I.L. Weissman, and S.J. Galli. 2005. Identification of mast cell progenitors in adult mice. *Proc. Natl. Acad. Sci. USA.* 102:11408–11413. http://dx.doi.org/10.1073/pnas.0504197102

Chen, P.P., J.R. Patel, I.N. Rybakova, J.W. Walker, and R.L. Moss. 2010. Protein kinase A-induced myofilament desensitization to Ca^{2+} as a result of phosphorylation of cardiac myosin-binding protein C. *J. Gen. Physiol.* 136:615–627. http://dx.doi.org/10.1085/jgp.201010448

Corvera, C.U., O. Déry, K. McConalogue, S.K. Böhm, L.M. Khitin, G.H. Caughey, D.G. Payan, and N.W. Bunnett. 1997. Mast cell tryptase regulates rat colonic myocytes through proteinase-activated receptor 2. *J. Clin. Invest.* 100:1383–1393. http://dx.doi.org/10.1172/JCI119658

Cousin, B., M. André, E. Arnaud, L. Pénicaud, and L. Casteilla. 2003. Reconstitution of lethally irradiated mice by cells isolated from adipose tissue. *Biochem. Biophys. Res. Commun.* 301:1016–1022. http://dx.doi.org /10.1016/S0006-291X(03)00061-5

Dahdah, A., G. Gautier, T. Attout, F. Fiore, E. Lebourdais, R. Msallam, M. Daëron, R.C. Monteiro, M. Benhamou, N. Charles, et al. 2014. Mast cells aggravate sepsis by inhibiting peritoneal macrophage phagocytosis. *J. Clin. Invest.* 124:4577–4589. http://dx.doi.org/10.1172/JCI75212

de Couto, G., W. Liu, E. Tseliou, B. Sun, N. Makkar, H. Kanazawa, M. Arditi, and E. Marbán. 2015. Macrophages mediate cardioprotective cellular postconditioning in acute myocardial infarction. *J. Clin. Invest.* 125:3147–3162. http://dx.doi.org/10.1172/JCI81321

Divoux, A., S. Moutel, C. Poitou, D. Lacasa, N. Veyrie, A. Aissat, M. Arock, M. Guerre-Millo, and K. Clément. 2012. Mast cells in human adipose tissue: link with morbid obesity, inflammatory status, and diabetes. *J. Clin. Endocrinol. Metab.* 97:E1677–E1685. http://dx.doi.org/10.1210/jc.2012 -1532

Dolgachev, V.A., M.R. Ullenbruch, N.W. Lukacs, and S.H. Phan. 2009. Role of stem cell factor and bone marrow-derived fibroblasts in airway remodeling. *Am. J. Pathol.* 174:390–400. http://dx.doi.org/10.2353/ ajpath.2009.080513

Dong, X., C.A. Sumandea, Y.C. Chen, M.L. Garcia-Cazarin, J. Zhang, C.W. Balke, M.P. Sumandea, and Y. Ge. 2012. Augmented phosphorylation of cardiac troponin I in hypertensive heart failure. *J. Biol. Chem.* 287:848– 857. http://dx.doi.org/10.1074/jbc.M111.293258

Dormishian, M., G. Turkeri, K. Urayama, T.L. Nguyen, M. Boulberdaa, N. Messaddeq, G. Renault, D. Henrion, and C.G. Nebigil. 2013. Prokineticin receptor-1 is a new regulator of endothelial insulin uptake and capillary formation to control insulin sensitivity and cardiovascular and kidney functions. *J. Am. Heart Assoc.* 2:e000411. http://dx.doi.org/10.1161/ JAHA.113.000411

Erdei, A., M. Andrásfalvy, H. Péterfy, G. Tóth, and I. Pecht. 2004. Regulation of mast cell activation by complement-derived peptides. *Immunol. Lett.* 92:39–42. http://dx.doi.org/10.1016/j.imlet.2003.11.019

Fauconnier, J., J. Thireau, S. Reiken, C. Cassan, S. Richard, S. Matecki, A.R. Marks, and A. Lacampagne. 2010. Leaky RyR2 trigger ventricular arrhythmias in Duchenne muscular dystrophy. *Proc. Natl. Acad. Sci. USA.* 107:1559–1564. http://dx.doi.org/10.1073/pnas.0908540107

Fazel, S., M. Cimini, L. Chen, S. Li, D. Angoulvant, P. Fedak, S. Verma, R.D. Weisel, A. Keating, and R.K. Li. 2006. Cardioprotective c-kit^{+} cells are from the bone marrow and regulate the myocardial balance of angiogenic cytokines. *J. Clin. Invest.* 116:1865–1877. http://dx.doi.org /10.1172/JCI27019

Feyerabend, T.B., A. Weiser, A. Tietz, M. Stassen, N. Harris, M. Kopf, P. Radermacher, P. Möller, C. Benoist, D. Mathis, et al. 2011. Cre-mediated cell ablation contests mast cell contribution in models of antibody- and T cell-mediated autoimmunity. *Immunity.* 35:832–844. http://dx.doi.org /10.1016/j.immuni.2011.09.015

Finley, N., M.B. Abbott, E. Abusamhadneh, V. Gaponenko, W. Dong, G. Gasmi-Seabrook, J.W. Howarth, M. Rance, R.J. Solaro, H.C. Cheung, and P.R. Rosevear. 1999. NMR analysis of cardiac troponin C-troponin I complexes: effects of phosphorylation. *FEBS Lett.* 453:107–112. http ://dx.doi.org/10.1016/S0014-5793(99)00693-6

Forman, M.F., G.L. Brower, and J.S. Janicki. 2006. Rat cardiac mast cell maturation and differentiation following acute ventricular volume

overload. *Inflamm. Res.* 55:408–415. http://dx.doi.org/10.1007/s00011-006-6016-z

Franco, C.B., C.C. Chen, M. Drukker, I.L. Weissman, and S.J. Galli. 2010. Distinguishing mast cell and granulocyte differentiation at the single-cell level. *Cell Stem Cell.* 6:361–368. http://dx.doi.org/10.1016/j.stem.2010.02.013

Frangogiannis, N.G., J.L. Perrard, L.H. Mendoza, A.R. Burns, M.L. Lindsey, C.M. Ballantyne, L.H. Michael, C.W. Smith, and M.L. Entman. 1998. Stem cell factor induction is associated with mast cell accumulation after canine myocardial ischemia and reperfusion. *Circulation.* 98:687–698. http://dx.doi.org/10.1161/01.CIR.98.7.687

Gorski, P.A., D.K. Ceholski, and R.J. Hajjar. 2015. Altered myocardial calcium cycling and energetics in heart failure--a rational approach for disease treatment. *Cell Metab.* 21:183–194. http://dx.doi.org/10.1016/j.cmet.2015.01.005

Grimbaldeston, M.A., C.C. Chen, A.M. Piliponsky, M. Tsai, S.Y. Tam, and S.J. Galli. 2005. Mast cell-deficient W-sash c-kit mutant Kit W-sh/W-sh mice as a model for investigating mast cell biology in vivo. *Am. J. Pathol.* 167:835–848. http://dx.doi.org/10.1016/S0002-9440(10)62055-X

Gruen, M., H. Prinz, and M. Gautel. 1999. cAPK-phosphorylation controls the interaction of the regulatory domain of cardiac myosin binding protein C with myosin-S2 in an on-off fashion. *FEBS Lett.* 453:254–259. http://dx.doi.org/10.1016/S0014-5793(99)00727-9

Guo, J., W. Jie, D. Kuang, J. Ni, D. Chen, Q. Ao, and G. Wang. 2009. Ischaemia/reperfusion induced cardiac stem cell homing to the injured myocardium by stimulating stem cell factor expression via NF-κB pathway. *Int. J. Exp. Pathol.* 90:355–364. http://dx.doi.org/10.1111/j.1365-2613.2009.00659.x

Gutierrez, D.A., S. Muralidhar, T.B. Feyerabend, S. Herzig, and H.R. Rodewald. 2015. Hematopoietic Kit deficiency, rather than lack of mast cells, protects mice from obesity and insulin resistance. *Cell Metab.* 21:678–691.

Han, J., Y.J. Koh, H.R. Moon, H.G. Ryoo, C.H. Cho, I. Kim, and G.Y. Koh. 2010. Adipose tissue is an extramedullary reservoir for functional hematopoietic stem and progenitor cells. *Blood.* 115:957–964. http://dx.doi.org/10.1182/blood-2009-05-219923

He, A., and G.P. Shi. 2013. Mast cell chymase and tryptase as targets for cardiovascular and metabolic diseases. *Curr. Pharm. Des.* 19:1114–1125. http://dx.doi.org/10.2174/1381612811319060012

Herron, T.J., F.S. Korte, and K.S. McDonald. 2001. Power output is increased after phosphorylation of myofibrillar proteins in rat skinned cardiac myocytes. *Circ. Res.* 89:1184–1190. http://dx.doi.org/10.1161/hh2401.101908

Janicki, J.S., G.L. Brower, and S.P. Levick. 2015. The emerging prominence of the cardiac mast cell as a potent mediator of adverse myocardial remodeling. *Methods Mol. Biol.* 1220:121–139. http://dx.doi.org/10.1007/978-1-4939-1568-2_8

Jiang, R., A. Zatta, H. Kin, N. Wang, J.G. Reeves, J. Mykytenko, J. Deneve, Z.Q. Zhao, R.A. Guyton, and J. Vinten-Johansen. 2007. PAR-2 activation at the time of reperfusion salvages myocardium via an ERK1/2 pathway in in vivo rat hearts. *Am. J. Physiol. Heart Circ. Physiol.* 293:H2845–H2852. http://dx.doi.org/10.1152/ajpheart.00209.2007

Katz, H.R., and K.F. Austen. 2011. Mast cell deficiency, a game of kit and mouse. *Immunity.* 35:668–670. http://dx.doi.org/10.1016/j.immuni.2011.11.004

Kirk, J.A., R.J. Holewinski, V. Kooij, G. Agnetti, R.S. Tunin, N. Witayavanitkul, P.P. de Tombe, W.D. Gao, J. Van Eyk, and D.A. Kass. 2014. Cardiac resynchronization sensitizes the sarcomere to calcium by reactivating GSK-3β. *J. Clin. Invest.* 124:129–139. http://dx.doi.org/10.1172/JCI69253

Kirshenbaum, A.S., J.P. Goff, S.W. Kessler, J.M. Mican, K.M. Zsebo, and D.D. Metcalfe. 1992. Effect of IL-3 and stem cell factor on the appearance of human basophils and mast cells from CD34+ pluripotent progenitor cells. *J. Immunol.* 148:772–777.

Kitamura, Y., S. Go, and K. Hatanaka. 1978. Decrease of mast cells in W/Wv mice and their increase by bone marrow transplantation. *Blood.* 52:447–452.

Kovanen, P.T. 2009. Mast cells in atherogenesis: actions and reactions. *Curr. Atheroscler. Rep.* 11:214–219. http://dx.doi.org/10.1007/s11883-009-0033-7

Kritikou, E., J. Kuiper, P.T. Kovanen, and I. Bot. 2016. The impact of mast cells on cardiovascular diseases. *Eur. J. Pharmacol.* 778:103–115. http://dx.doi.org/10.1016/j.ejphar.2015.04.050

Kulikovskaya, I., G. McClellan, R. Levine, and S. Winegrad. 2003. Effect of extraction of myosin binding protein C on contractility of rat heart. *Am. J. Physiol. Heart Circ. Physiol.* 285:H857–H865. http://dx.doi.org/10.1152/ajpheart.00841.2002

Kumar, D., T.A. Hacker, J. Buck, L.F. Whitesell, E.H. Kaji, P.S. Douglas, and T.J. Kamp. 2005. Distinct mouse coronary anatomy and myocardial infarction consequent to ligation. *Coron. Artery Dis.* 16:41–44. http://dx.doi.org/10.1097/00019501-200502000-00008

Layland, J., R.J. Solaro, and A.M. Shah. 2005. Regulation of cardiac contractile function by troponin I phosphorylation. *Cardiovasc. Res.* 66:12–21. http://dx.doi.org/10.1016/j.cardiores.2004.12.022

Levine, R., A. Weisberg, I. Kulikovskaya, G. McClellan, and S. Winegrad. 2001. Multiple structures of thick filaments in resting cardiac muscle and their influence on cross-bridge interactions. *Biophys. J.* 81:1070–1082. http://dx.doi.org/10.1016/S0006-3495(01)75764-5

Li, M.X., X. Wang, and B.D. Sykes. 2004. Structural based insights into the role of troponin in cardiac muscle pathophysiology. *J. Muscle Res. Cell Motil.* 25:559–579. http://dx.doi.org/10.1007/s10974-004-5879-2

Liu, J., A. Divoux, J. Sun, J. Zhang, K. Clément, J.N. Glickman, G.K. Sukhova, P.J. Wolters, J. Du, C.Z. Gorgun, et al. 2009. Genetic deficiency and pharmacological stabilization of mast cells reduce diet-induced obesity and diabetes in mice. *Nat. Med.* 15:940–945. http://dx.doi.org/10.1038/nm.1994

Ludeman, M.J., Y.W. Zheng, K. Ishii, and S.R. Coughlin. 2004. Regulated shedding of PAR1 N-terminal exodomain from endothelial cells. *J. Biol. Chem.* 279:18592–18599. http://dx.doi.org/10.1074/jbc.M310836200

Manni, S., J.H. Mauban, C.W. Ward, and M. Bond. 2008. Phosphorylation of the cAMP-dependent protein kinase (PKA) regulatory subunit modulates PKA-AKAP interaction, substrate phosphorylation, and calcium signaling in cardiac cells. *J. Biol. Chem.* 283:24145–24154. http://dx.doi.org/10.1074/jbc.M802278200

Matsuzawa, S., K. Sakashita, T. Kinoshita, S. Ito, T. Yamashita, and K. Koike. 2003. IL-9 enhances the growth of human mast cell progenitors under stimulation with stem cell factor. *J. Immunol.* 170:3461–3467. http://dx.doi.org/10.4049/jimmunol.170.7.3461

McLarty, J.L., G.C. Meléndez, G.L. Brower, J.S. Janicki, and S.P. Levick. 2011. Tryptase/protease-activated receptor 2 interactions induce selective mitogen-activated protein kinase signaling and collagen synthesis by cardiac fibroblasts. *Hypertension.* 58:264–270. http://dx.doi.org/10.1161/HYPERTENSIONAHA.111.169417

McLean, P.G., D. Aston, D. Sarkar, and A. Ahluwalia. 2002. Protease-activated receptor-2 activation causes EDHF-like coronary vasodilation: selective preservation in ischemia/reperfusion injury: involvement of lipoxygenase products, VR1 receptors, and C-fibers. *Circ. Res.* 90:465–472. http://dx.doi.org/10.1161/hh0402.105372

Movsesian, M. 2015. New pharmacologic interventions to increase cardiac contractility: challenges and opportunities. *Curr. Opin. Cardiol.* 30:285–291. http://dx.doi.org/10.1097/HCO.0000000000000165

Murray, D.B., J. McLarty-Williams, K.T. Nagalla, and J.S. Janicki. 2012. Tryptase activates isolated adult cardiac fibroblasts via protease activated receptor-2 (PAR-2). *J. Cell Commun. Signal.* 6:45–51. http://dx.doi.org/10.1007/s12079-011-0146-y

Napoli, C., C. Cicala, J.L. Wallace, F. de Nigris, V. Santagada, G. Caliendo, F. Franconi, L.J. Ignarro, and G. Cirino. 2000. Protease-activated receptor-2 modulates myocardial ischemia-reperfusion injury in the rat heart. *Proc. Natl. Acad. Sci. USA.* 97:3678–3683. http://dx.doi.org/10.1073/pnas.97.7.3678

Nixon, B.R., S.D. Walton, B. Zhang, E.A. Brundage, S.C. Little, M.T. Ziolo, J.P. Davis, and B.J. Biesiadecki. 2014. Combined troponin I Ser-150 and Ser-23/24 phosphorylation sustains thin filament Ca^{2+} sensitivity and accelerates deactivation in an acidic environment. *J. Mol. Cell. Cardiol.* 72:177–185. http://dx.doi.org/10.1016/j.yjmcc.2014.03.010

Oka, T., J. Kalesnikoff, P. Starkl, M. Tsai, and S.J. Galli. 2012. Evidence questioning cromolyn's effectiveness and selectivity as a 'mast cell stabilizer' in mice. *Lab. Invest.* 92:1472–1482. http://dx.doi.org/10.1038/labinvest.2012.116

Okada, M., H. Tokumitsu, Y. Kubota, and R. Kobayashi. 2002. Interaction of S100 proteins with the antiallergic drugs, olopatadine, amlexanox, and cromolyn: identification of putative drug binding sites on S100A1 protein. *Biochem. Biophys. Res. Commun.* 292:1023–1030. http://dx.doi.org/10.1006/bbrc.2002.6761

Okada, M., H. Itoh, T. Hatakeyama, H. Tokumitsu, and R. Kobayashi. 2003. Hsp90 is a direct target of the anti-allergic drugs disodium cromoglycate and amlexanox. *Biochem. J.* 374:433–441. http://dx.doi.org/10.1042/bj20030351

Oliveira, S.H., D.D. Taub, J. Nagel, R. Smith, C.M. Hogaboam, A. Berlin, and N.W. Lukacs. 2002. Stem cell factor induces eosinophil activation and degranulation: mediator release and gene array analysis. *Blood.* 100:4291–4297. http://dx.doi.org/10.1182/blood.V100.13.4291

Poglio, S., F. De Toni-Costes, E. Arnaud, P. Laharrague, E. Espinosa, L. Casteilla, and B. Cousin. 2010. Adipose tissue as a dedicated reservoir of functional mast cell progenitors. *Stem Cells.* 28:2065–2072. http://dx.doi.org/10.1002/stem.523

Poglio, S., F. De Toni, D. Lewandowski, A. Minot, E. Arnaud, V. Barroca, P. Laharrague, L. Casteilla, and B. Cousin. 2012. In situ production of innate immune cells in murine white adipose tissue. *Blood.* 120:4952–4962. http://dx.doi.org/10.1182/blood-2012-01-406959

Rababa'h, A., S. Singh, S.V. Suryavanshi, S.E. Altarabsheh, S.V. Deo, and B.K. McConnell. 2015. Compartmentalization role of A-kinase anchoring proteins (AKAPs) in mediating protein kinase A (PKA) signaling and cardiomyocyte hypertrophy. *Int. J. Mol. Sci.* 16:218–229. http://dx.doi.org/10.3390/ijms16010218

Rajagopal, S., K. Rajagopal, and R.J. Lefkowitz. 2010. Teaching old receptors new tricks: biasing seven-transmembrane receptors. *Nat. Rev. Drug Discov.* 9:373–386. http://dx.doi.org/10.1038/nrd3024

Ramirez-Correa, G.A., S. Cortassa, B. Stanley, W.D. Gao, and A.M. Murphy. 2010. Calcium sensitivity, force frequency relationship and cardiac troponin I: critical role of PKA and PKC phosphorylation sites. *J. Mol. Cell. Cardiol.* 48:943–953. http://dx.doi.org/10.1016/j.yjmcc.2010.01.004

Reid, A.C., J.A. Brazin, C. Morrey, R.B. Silver, and R. Levi. 2011. Targeting cardiac mast cells: pharmacological modulation of the local renin-angiotensin system. *Curr. Pharm. Des.* 17:3744–3752. http://dx.doi.org/10.2174/138161211798357908

Schmetzer, O., P. Valentin, M.K. Church, M. Maurer, and F. Siebenhaar. 2016. Murine and human mast cell progenitors. *Eur. J. Pharmacol.* 778:2–10. http://dx.doi.org/10.1016/j.ejphar.2015.07.016

Shpacovitch, V.M., T. Brzoska, J. Buddenkotte, C. Stroh, C.P. Sommerhoff, J.C. Ansel, K. Schulze-Osthoff, N.W. Bunnett, T.A. Luger, and M. Steinhoff. 2002. Agonists of proteinase-activated receptor 2 induce cytokine release

and activation of nuclear transcription factor kappaB in human dermal microvascular endothelial cells. *J. Invest. Dermatol.* 118:380–385. http://dx.doi.org/10.1046/j.0022-202x.2001.01658.x

Solaro, R.J., and G.M. Arteaga. 2007. Heart failure, ischemia/reperfusion injury and cardiac troponin. *Adv. Exp. Med. Biol.* 592:191–200. http://dx.doi.org/10.1007/978-4-431-38453-3_17

Somasundaram, P., G. Ren, H. Nagar, D. Kraemer, L. Mendoza, L.H. Michael, G.H. Caughey, M.L. Entman, and N.G. Frangogiannis. 2005. Mast cell tryptase may modulate endothelial cell phenotype in healing myocardial infarcts. *J. Pathol.* 205:102–111. http://dx.doi.org/10.1002/path.1690

Sriwai, W., S. Mahavadi, O. Al-Shboul, J.R. Grider, and K.S. Murthy. 2013. Distinctive G protein-dependent signaling by protease-activated receptor 2 (PAR2) in smooth muscle: Feedback inhibition of RhoA by cAMP-independent PKA. *PLoS One.* 8:e66743. http://dx.doi.org/10.1371/journal.pone.0066743

Stelzer, J.E., J.R. Patel, J.W. Walker, and R.L. Moss. 2007. Differential roles of cardiac myosin-binding protein C and cardiac troponin I in the myofibrillar force responses to protein kinase A phosphorylation. *Circ. Res.* 101:503–511. http://dx.doi.org/10.1161/CIRCRESAHA.107.153650

Sumandea, C.A., M.L. Garcia-Cazarin, C.H. Bozio, G.A. Sievert, C.W. Balke, and M.P. Sumandea. 2011. Cardiac troponin T, a sarcomeric AKAP, tethers protein kinase A at the myofilaments. *J. Biol. Chem.* 286:530–541. http://dx.doi.org/10.1074/jbc.M110.148684

Sykes, B.D. 2003. Pulling the calcium trigger. *Nat. Struct. Biol.* 10:588–589. http://dx.doi.org/10.1038/nsb0803-588

Tallini, Y.N., K.S. Greene, M. Craven, A. Spealman, M. Breitbach, J. Smith, P.J. Fisher, M. Steffey, M. Hesse, R.M. Doran, et al. 2009. c-kit expression identifies cardiovascular precursors in the neonatal heart. *Proc. Natl. Acad. Sci. USA.* 106:1808–1813. http://dx.doi.org/10.1073/pnas.0808920106

Thoemmes, S.F., C.A. Stutzke, Y. Du, M.D. Browning, P.M. Buttrick, and L.A. Walker. 2014. Characterization and validation of new tools for measuring site-specific cardiac troponin I phosphorylation. *J. Immunol. Methods.* 403:66–71. http://dx.doi.org/10.1016/j.jim.2013.11.020

Toeg, H.D., R. Tiwari-Pandey, R. Seymour, A. Ahmadi, S. Crowe, B. Vulesevic, E.J. Suuronen, and M. Ruel. 2013. Injectable small intestine submucosal extracellular matrix in an acute myocardial infarction model. *Ann. Thorac. Surg.* 96:1686–1694. http://dx.doi.org/10.1016/j.athoracsur.2013.06.063

Tran, T.T., and C.R. Kahn. 2010. Transplantation of adipose tissue and stem cells: role in metabolism and disease. *Nat. Rev. Endocrinol.* 6:195–213. http://dx.doi.org/10.1038/nrendo.2010.20

Trejo, J., A.J. Connolly, and S.R. Coughlin. 1996. The cloned thrombin receptor is necessary and sufficient for activation of mitogen-activated protein kinase and mitogenesis in mouse lung fibroblasts. Loss of responses in fibroblasts from receptor knockout mice. *J. Biol. Chem.* 271:21536–21541. http://dx.doi.org/10.1074/jbc.271.35.21536

Ward, D.G., S.M. Brewer, M.P. Cornes, and I.P. Trayer. 2003. A cross-linking study of the N-terminal extension of human cardiac troponin I. *Biochemistry.* 42:10324–10332. http://dx.doi.org/10.1021/bi034495r

Weithauser, A., and U. Rauch. 2014. Role of protease-activated receptors for the innate immune response of the heart. *Trends Cardiovasc. Med.* 24:249–255. http://dx.doi.org/10.1016/j.tcm.2014.06.004

Welker, P., J. Grabbe, T. Zuberbier, S. Guhl, and B.M. Henz. 2000. Mast cell and myeloid marker expression during early in vitro mast cell differentiation from human peripheral blood mononuclear cells. *J. Invest. Dermatol.* 114:44–50. http://dx.doi.org/10.1046/j.1523-1747.2000.00827.x

Wernersson, S., and G. Pejler. 2014. Mast cell secretory granules: armed for battle. *Nat. Rev. Immunol.* 14:478–494. http://dx.doi.org/10.1038/nri3690

White, H.D., and D.P. Chew. 2008. Acute myocardial infarction. *Lancet.* 372:570–584. http://dx.doi.org/10.1016/S0140-6736(08)61237-4

White, H.D., K. Thygesen, J.S. Alpert, and A.S. Jaffe. 2014. Republished: clinical implications of the third universal definition of myocardial infarction. *Postgrad. Med. J.* 90:502–510. http://dx.doi.org/10.1136/postgradmedj-2012-302976rep

Xaubet, A., J.A. Moisés, C. Agustí, J.A. Martos, and C. Picado. 1991. Identification of mast cells in bronchoalveolar lavage fluid. Comparison between different fixation and staining methods. *Allergy.* 46:222–227. http://dx.doi.org/10.1111/j.1398-9995.1991.tb00575.x

Xiang, F.L., X. Lu, Y. Liu, and Q. Feng. 2013. Cardiomyocyte-specific overexpression of human stem cell factor protects against myocardial ischemia and reperfusion injury. *Int. J. Cardiol.* 168:3486–3494. http://dx.doi.org/10.1016/j.ijcard.2013.04.165

Yang, Y., J.Y. Lu, X. Wu, S. Summer, J. Whoriskey, C. Saris, and J.D. Reagan. 2010. G-protein-coupled receptor 35 is a target of the asthma drugs cromolyn disodium and nedocromil sodium. *Pharmacology.* 86:1–5. http://dx.doi.org/10.1159/000314164

Zhang, T., D.F. Finn, J.W. Barlow, and J.J. Walsh. 2016. Mast cell stabilisers. *Eur. J. Pharmacol.* 778:158–168. http://dx.doi.org/10.1016/j.ejphar.2015.05.071

Zhong, B., and D.H. Wang. 2009. Protease-activated receptor 2-mediated protection of myocardial ischemia-reperfusion injury: role of transient receptor potential vanilloid receptors. *Am. J. Physiol. Regul. Integr. Comp. Physiol.* 297:R1681–R1690. http://dx.doi.org/10.1152/ajpregu.90746.2008

Zouggari, Y., H. Ait-Oufella, P. Bonnin, T. Simon, A.P. Sage, C. Guérin, J. Vilar, G. Caligiuri, D. Tsiantoulas, L. Laurans, et al. 2013. B lymphocytes trigger monocyte mobilization and impair heart function after acute myocardial infarction. *Nat. Med.* 19:1273–1280. http://dx.doi.org/10.1038/nm.3284

1374

The role of mast cells in myocardial infarction | Ngkelo et al.